Best Available Copy

AD

AD643538

NDL-TR-68

SCATTERED RADIATION (SKYSHINE) CONTRIBUTION TO AN OPEN BASEMENT LOCATED IN A SIMULATED FALLOUT FIELD

FINAL REPORT

by

Michael J. Schumchyk
Murray A. Schmoke
Walter O. Egerland
Ernest L. Schulman

For

Office of Civil Defense
Office of the Secretary of the Army
Washington, D. C. 20310

OCD Work Order OCD-PS-64-91, Subtask 1111F

DECEMBER 1966

BEST AVAILABLE COPY

BEST AVAILABLE COPY

US ARMY
NUCLEAR DEFENSE LABORATORY
EDGEWOOD ARSENAL, MARYLAND

Disposition

Destroy this report when no longer needed. Do not return it to the originator.

Disclaimer

The findings in this report are not to be construed as an official Department of the Army position.

Trade Names

Citation of trade names in this report does not constitute an official Department of the Army endorsement or approval of the use of such commercial items.

NDL-TR-68

SCATTERED RADIATION (SKYSHINE) CONTRIBUTION TO AN OPEN BASEMENT LOCATED IN A SIMULATED FALLOUT FIELD

Final Report

by

Michael J. Schumchyk
Murray A. Schmoke
Walter O. Egerland
Ernest L. Schulman

for

Office of Civil Defense
Office of the Secretary of the Army
Washington, D.C. 20310

OCD Work Order OCD-PS-64-91, Subtask 1111F

December 1966

OCD REVIEW NOTICE

This report has been reviewed in the Office of Civil Defense and approved for publication. Approval does not signify that the contents necessarily reflect the views and policies of the Office of Civil Defense.

Distribution of this document is unlimited.

US ARMY
NUCLEAR DEFENSE LABORATORY
Edgewood Arsenal, Maryland

ABSTRACT

The objective of this work was to determine, experimentally, the shielding afforded by an open, concrete-walled basement located in a simulated fallout field and to compare these experimental results with theoretical results published in National Bureau of Standards (NBS) Monograph 42.

A cobalt-60 point-source circulation system was used to simulate a uniformly-contaminated residual gamma radiation area out to a radius of 600 feet. Experimental exposure-rate measurements were made in the free field and at various locations within the structure as a function of height above the basement floor. Ionization chamber dosimeters were used as radiation detectors. Experimental measurements were extrapolated to infinite-field conditions by use of analytical procedures and compared with other related experimental data and theoretical results.

The following conclusions were established:

(1) Analysis of the position function $f(h,\omega)$ at various detector levels above the basement floor indicates the presence of radiation backscattering contribution that is dependent on height above the floor and solid-angle fraction and is not adequately estimated by a single correction factor (1.2 suggested in NBS Monograph 42).

(2) Agreement within 21 percent was obtained between experimental reduction factors and theoretical reduction factors calculated by Equation 31.1 of NBS Monograph 42 for detector locations in the center or near the center of the basement (detector locations C and B).

(3) Theoretical reduction factors underestimate experimental reduction factors at the off-center detector locations close to the basement walls (detector locations A, D, and E) by as much as 47 percent. The differences appear to be caused by radiation scattered from the walls and floor of the basement; this scattering is not completely accounted for in the theoretical calculations.

(4) Extrapolation to the ground surface ($\omega = 1$) of the experimentally measured reduction factors at the center detector location within the open concrete basement yields a skyshine exposure rate that is 7.9 percent of the infinite free-field exposure rate at the 3-foot height. This compares favorably with 8.8 percent calculated in the NBS Monograph 42.

(5) The infinite-field exposure rate at the 3-foot height above a graded, rolled, and relatively smooth field was determined as 468 R/h at a source density of 1 Ci/ft^2 of cobalt-60 radiation simulated with a circulating point source.

FOREWORD

The work described herein was accomplished under OCD Work Order No. OCD-PS-64-91, Subtask No. 1111F, and DASA NWER Subtask No. 11.008.

The authors wish to express their appreciation to Mr. Charles Eisenhauer of the National Bureau of Standards for his technical comments and suggestions during the experimental phase of the project.

CONTENTS

SCATTERED RADIATION (SKYSHINE) CONTRIBUTION TO AN OPEN BASEMENT LOCATED IN A SIMULATED FALLOUT FIELD

1. INTRODUCTION

This report, fourth in a series (References 1, 2, 3), presents further progress in the US Army Nuclear Defense Laboratory (USANDL) experimental shielding program to test the validity of theoretical calculations for predicting the protection afforded by structures against fallout radiation.

1.1 Objective.

The objective of this subtask was to determine, experimentally, the shielding provided by an open, concrete-walled basement located in a simulated fallout field, and to compare the results of this experiment with theoretical results of National Bureau of Standards (NBS) Monograph 42 (Reference 4).

1.2 Background.

L. V. Spencer of NBS developed a prediction method for determining the shielding effectiveness of structures located in actual or simulated fallout fields. This method, described in Reference 4, became the basis for the engineering manual (Reference 5) published by the Office of Civil Defense (OCD). The manual is used by engineers, architects, and military commanders to predict the protection afforded by existing and proposed structures against fallout gamma radiation.

The information in NBS 42 has been obtained almost completely by machine calculations utilizing basic cross-section data. A number of sources of experimental data are mentioned, but detailed comparisons with such data are not included. This prediction method has been tested experimentally, first with simple structures and then with more complex structures. This Laboratory has conducted experiments with a simple concrete blockhouse, located in a simulated fallout field, to determine the effect of roof thickness and wall thickness on the attenuation of gamma radiation (References 2 and 3). Radiation-penetration measurements for the roof indicated agreement within 20 percent between experimental and theoretical reduction factors determined along the vertical center line of the structure. Experimental and theoretical reduction factors for the wall of the structure agreed within 15 percent at 3 feet and 6 feet above the center of the structure. However, little experimental work has been done on basement structures.

Some experimental work measuring "skyshine" radiation was done by Clifford (Reference 6), who measured the radiation penetration in a circular foxhole from a residual radiation area simulated with cesium-137 sources. Starbird and Batter also measured the radiation penetration in a circular foxhole, but used cobalt-60 sources to simulate the residual radiation area (Reference 7).

More recent work with the circular foxhole and cobalt-60 sources has been performed by Burson and Summers in the Nevada desert (Reference 8). Extensive measurements were made both in the open hole and in the covered hole with various materials.

The work reported here is concerned with measuring air-scattered (skyshine) radiation penetration into what might be considered a full-scale open basement. All experimental data are given in Appendix A.

2. PROCEDURES

2.1 Test Area.

The experiment was conducted at the USANDL Westwood test area comprising approximately 60 acres, of which 24 acres have been cleared. The surface of the simulated radiation area was a sandy clay that had been graded, rolled, and treated with a herbicide to prevent the growth of grass. The entire area was enclosed by a 6-foot-high fence equipped with a pressure-sensitive personnel alarm. A field office on the test site provided a place to charge and read dosimeters. The office was shielded from the radiation field by a 32-inch-thick concrete wall. This wall reduced the radiation sufficiently to allow test personnel to remain in the building during testing.

2.2 Source-Handling Facility.

A point-source circulation system was used to simulate fallout radiation (Reference 9). The simulation system involved the placement of nylon tubing, 1/16-inch wall thickness and 3/8-inch diameter, in a uniform pattern on the ground around the structure. A radioactive point source was then propelled by water pressure through the tubing at a constant speed to simulate a uniform distribution of contamination over the area. Since the sources were calibrated within the tubing, no correction was made for energy degradation of the source due to the tubing.

Nylon tubing was placed in a 600-foot-radius semicircular array consisting of four semiannuli (Figure 2.1). The spacing between rows of tubing, inner and outer radial distances of each semiannulus, and area of each semiannulus, are shown in Table 2.1.

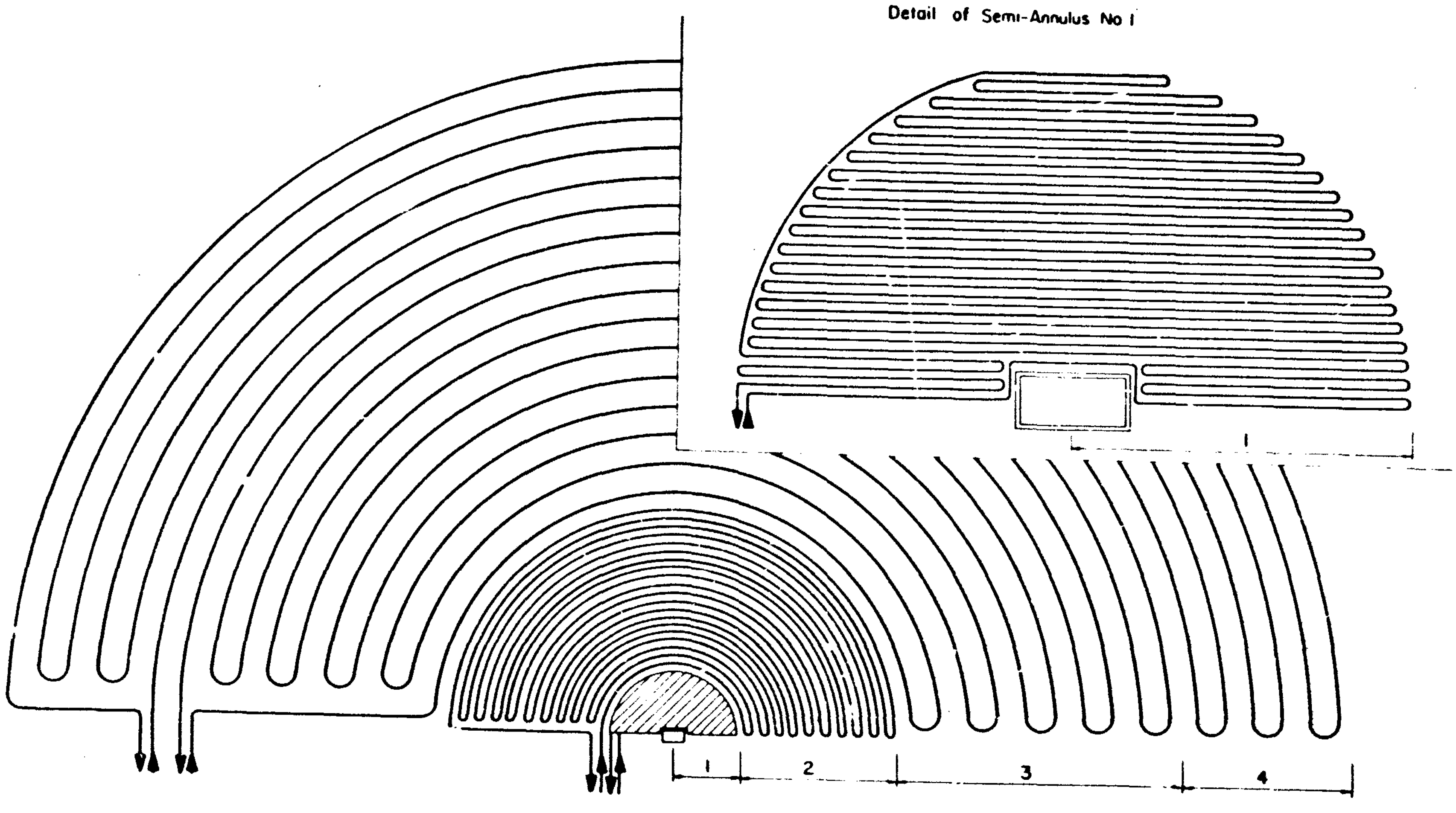

Semi-Annulus No	Inner and Outer Radius (ft)	Tube Spacing (ft)
1	0 – 60	1.67
2	60 – 200	7
3	200 – 450	25
4	450 – 600	25

Figure 2.1 Semicircular array of nylon tubing.

TABLE 2.1 DESCRIPTION OF SEMICIRCULAR TUBING ARRAY

Semiannulus	Tube Spacing	Inner and Outer Radial Distance	Semiannular Area
	ft	ft	ft^2
1	1.67	0 to 60	5,499
2	7.0	60 to 200	57,177
3	25	200 to 450	255,255
4	25	450 to 600	247,401

2.3 Sources.

Six cobalt-60 sources (18.5 curies, 53.4 curies, 94.5 curies, 185 curies, 332 curies, and 590 curies) were used in this experiment. Calibration date of these sources was 1 March 1962. The choice of a source for a particular test was based upon relative sensitivity of the radiation detectors, source-to-detector distance, and exposure time. All sources were calibrated against a source that had been calibrated in the free air at a height of 11 feet. Victoreen condenser-R-Chambers, calibrated by NBS, were used to obtain three measurements for each source exposure. All readings were within 2 percent of the average for a particular source. Recalibration of these sources was performed 1 September 1964 by the method described in Appendix B. Radioactive decay corrections were made on the experimental data.

Dimensional replicas of the radioactive sources (cobalt-60 pellets doubly encapsulated in stainless steel) are shown on the left side of Figure 2.2. The capsule was crimped to the end of a flexible stainless-steel cable. The leader, connected to the other end of the cable, held a 1/2-inch-diameter leather skirt. The leather skirt acted as a piston by providing a seal between the source assembly and the wall surface of the tubing to permit the propulsion of the source assembly by water pressure.

2.4 Instrumentation.

Radiation-dose measurements were made with the following Victoreen ionization chamber dosimeters: Model 208, 1 mR; Model 239, 10 mR; and Model 362, 200 mR. A Victoreen Model 287 charger-reader was used to charge and read dosimeters. Dosimeter selection was based upon the exposure time, the

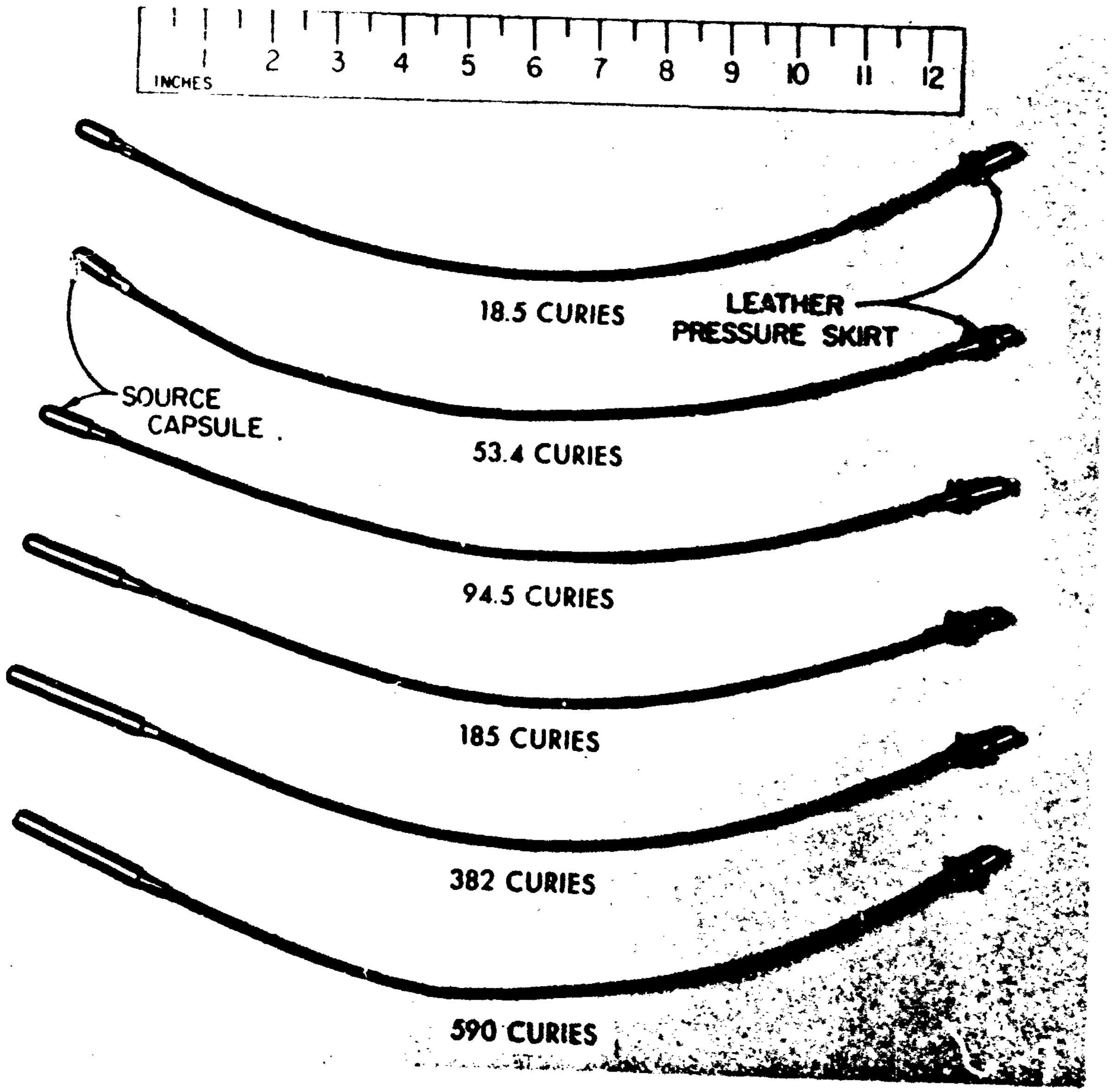

Figure 2.2 Dimensional replicas of cobalt-60 radioactive sources with leaders.

section of the field being simulated, and the location of the dosimeters with respect to the contaminated area. The choice of dosimeters was such that the dose received was about mid-scale on the charger-reader. Experience with the dosimeters indicated that mid-scale deflections could be reproduced within ±2 percent. Each exposure was timed by a Precision Instrument Company electric timer.

The ionization-chamber dosimeters were calibrated against a Victoreen Model 130 R-Chamber (0.25R) and charged and read on a Victoreen Model 70-R meter. The R-meter and R-chamber were calibrated by NBS with a collimated beam of cobalt-60 gamma rays. The estimated accuracy of the NBS calibration was ±3 percent.

2.5 Description of Experimental Structure.

The rectangular basement, with walls of reinforced concrete, is shown in perspective with tubing layout in Figure 2.3. The inside dimensions of the structure were 20 by 10 by 7 feet. The poured concrete walls were 20 inches thick and the floor was 3 inches thick.

The relatively thick concrete walls were built to serve as a foundation for aboveground walls for future experiments and to prevent any ground direct radiation (lip contribution) from reaching the detectors in the basement. Note the inset in Figure 2.1, an enlargement of semiannulus 1 adjacent to the basement, which shows that the first line of tubing is 10 inches from the concrete wall. In this position direct radiation must penetrate approximately 10 mean free paths of concrete to reach the nearest detector; therefore, it was concluded that the lip contribution was effectively eliminated by the walls.

2.6 Experimental Technique.

Exposure-rate reduction factors within the test structure were obtained by determining the ratio D/D_o, where D is the exposure rate measured in the structure and D_o is the exposure rate measured in the free field at 3 feet above the center of a contaminated infinite field.

Free-field radiation exposure measurements were made at heights from 1 to 15 feet above ground at 1-foot intervals. Although only the 3-foot detector height data were required to calculate the experimental reduction factors for comparison with theoretical reduction factors, data for other heights were taken so that comparisons could be made with similar data taken by other investigators (Reference 10), and with the theoretical L(d) curve of Spencer. These comparisons allow some estimate to be made of the ground roughness effects on radiation intensity.

Free-field measurements were made with the detector stand mounted directly above the center of the basement for semiannuli 2, 3, and 4. Free-field measurements for semiannulus 1 (see inset Figure 2.1) were made over a

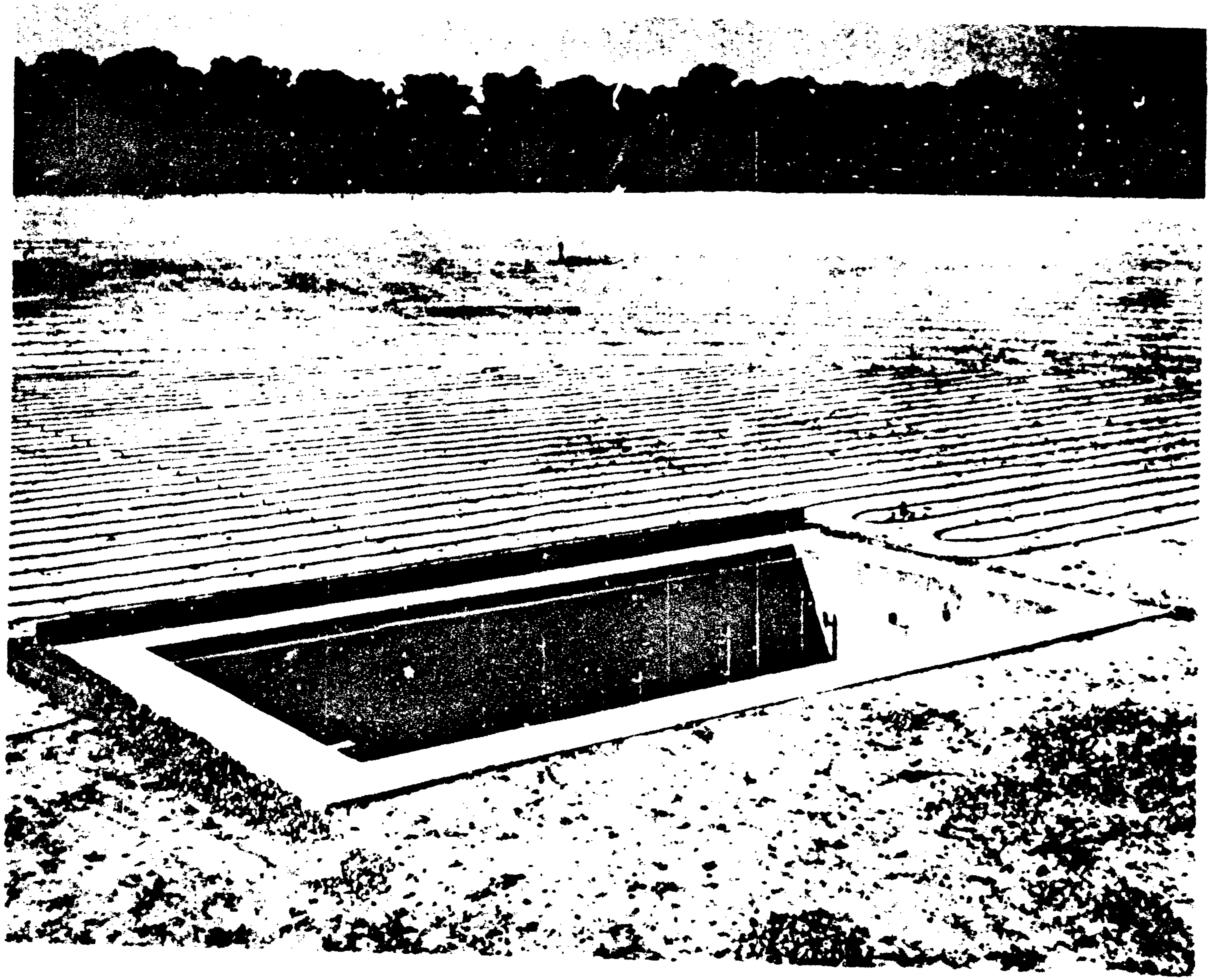

Figure 2.3 Basement structure showing tubing layout and masonite water deflector.

separate semiannulus with tubing laid out to cover the entire radius of the semiannulus, which was offset 300 feet from the basement over graded, level terrain. The total free-field measurements listed in Table 3.1 are for the entire field and not for an area with a portion of the contamination cleared away at the center.

The detector stand resembled a gibbet with a 2 1/2-foot long horizontal arm braced at the top of an 18-foot high vertical support (wooden four-by-four). The detector holders were paper cups taped to two parallel 1/16-inch diameter stainless steel wires attached at the end of the horizontal arm and anchored at the base of the gibbet by a 30-pound lead brick. The entire assembly was supported by three guy wires and adjusted so that the line of detectors was perpendicular to the center point of the diameter of the semiannulus. Ten source runs were made for each semiannular area and the exposure measurements were checked for reproducibility.

The detector layout inside the basement structure is shown in Figure 2.4, a cross-section view of the detector positions with respect to the floor, and in Figure 2.5, a plan view of the location of the detectors with respect to the walls of the building. Primary detectors (capital letters) and image detectors (small letters) were placed within the structure as shown in Figure 2.5. To obtain the total radiation exposure from the simulated fallout area for detector locations A, B, and E, the exposure rate at the primary positions A, B, and E were added to the exposure rate at the image positions a, b, and e, respectively. At each detector height for detector locations C and D, the exposures were doubled.

All exposure measurements were converted to milliroentgens per hour for a source density of 1 Ci/ft^2 by use of the following equation:

$$D = D_x A \frac{\rho \lambda C}{S} , \qquad (2.1)$$

where

D = the corrected exposure rate in $(mR/h)/(Ci/ft^2)$,

D_x = the uncorrected exposure rate in (mR/h),

A = the area of the semiannulus in ft^2

ρ = the atmospheric correction factor at standard conditions (described below),

λ = decay factor for cobalt 60 used to correct the exposure reading to a reference time,

C = the calibration factor of a given detector, and

S = the strength in curies.

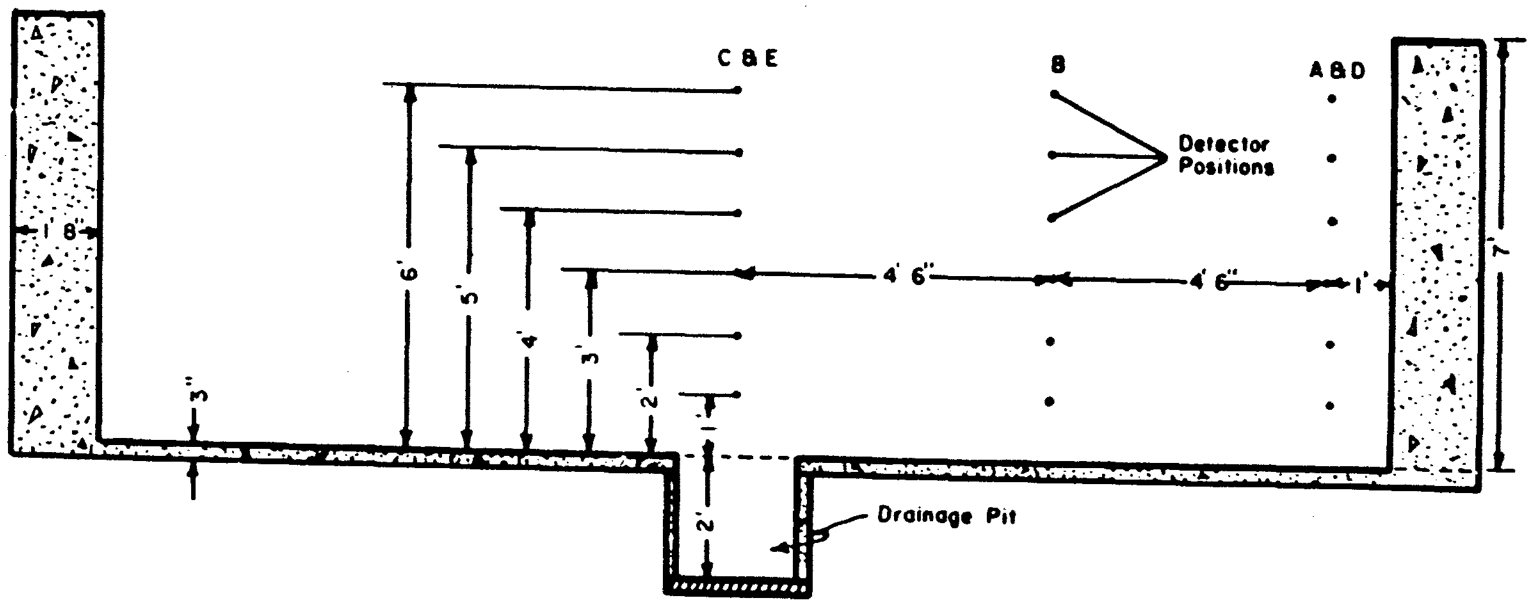

Figure 2.4 Basement section showing elevation of detector locations.

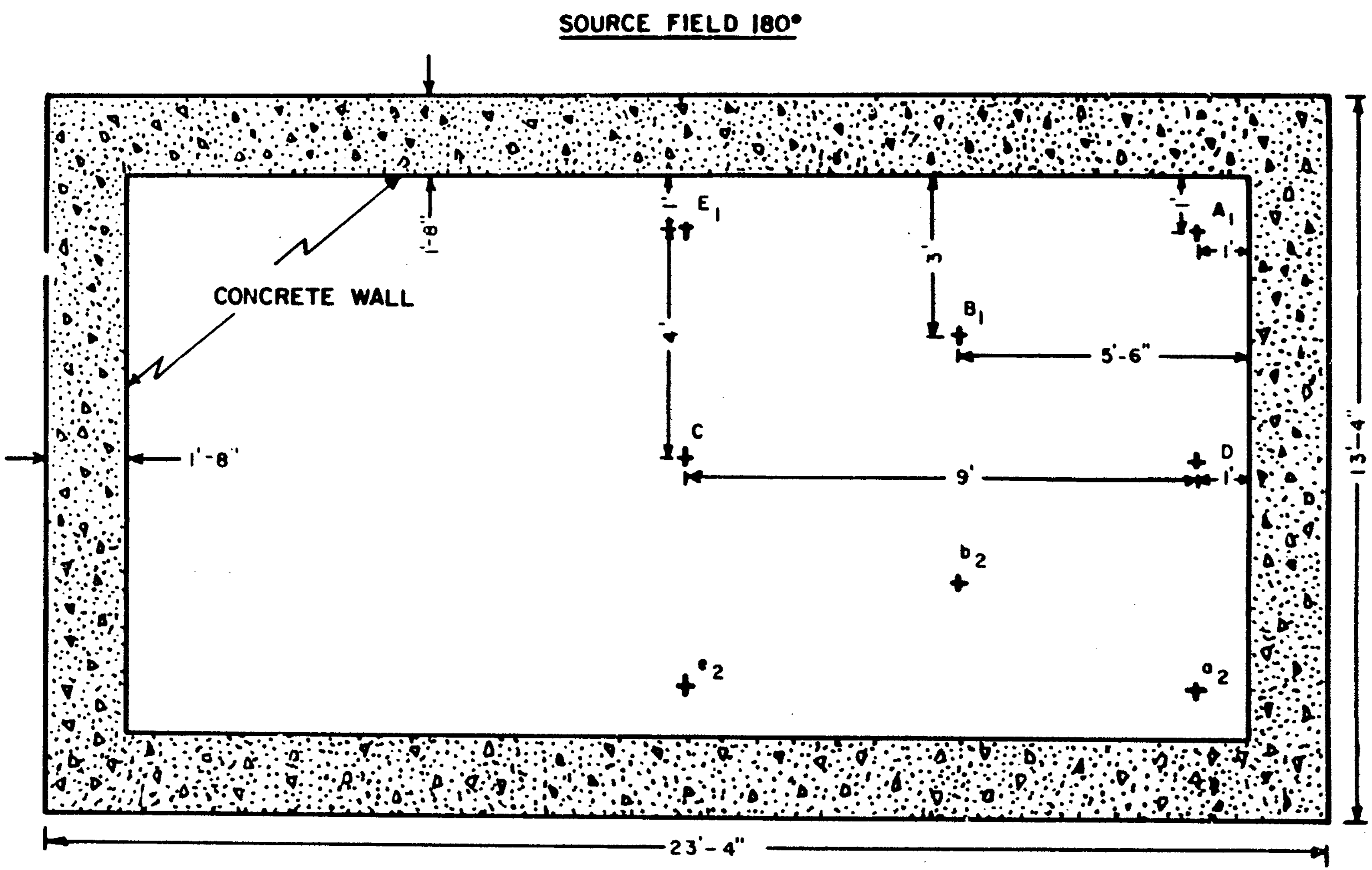

Figure 2.5 Basement plan of primary and image detector locations.

2.7 Discussion of Errors.

To estimate the error in most laboratory-type experiments, a large number of experimental runs are usually made, from which the standard deviation, σ, is calculated. The reliability of the estimated error is dependent on the number of experimental runs, N. However, in a field-type experiment this is usually not possible nor practical. In this experiment, the time required to make a large number of runs on each semiannulus would have been excessive. To compensate for this, attempts were made to carefully control the factors that could produce experimental variation and to analyze the systematic errors which are inherent when different personnel charge and read the ionization chamber dosimeters.

A point-source circulation system, in which a source of cobalt 60 was propelled through plastic tubing at a constant rate, was used to simulate residual radiation. Since the system depends on the source remaining the same amount of time in a given area of the field, an error could result if there were lack of uniformity of movement of the source through the tubing. To minimize this possibility, a "dummy source," an exact replica of the actual source, was propelled through the tubing prior to the "hot" run. The movement of the dummy source was observed to determine whether any imperfections in the tubing or any variations in the pumping system were present to cause irregular flow of the source. Any delay in the flow would increase the total time of a run. Results of this pre-testing showed that the variation in the times for the experimental runs would never be greater than 0.5 percent for a given semiannulus. Since all measurements were normalized to milliroentgens per hour, the error in timing would be averaged out in the normalization.

Further experimental error could be caused by errors in source calibration. All sources were calibrated on the USANDL calibration range, as described in Appendix B. The calibration error, σ_1, calculated from five repetitive measurements for each source was no greater than ± 2 percent.

The ionization chamber dosimeters that were used to make the exposure measurements are the most sensitive to possible error. Error could result from variations in temperature, pressure, leakage, and reading. Since the ionization chambers were not hermetically sealed and the ionization of the air within the chambers is dependent to some extent on the air density, the chambers are sensitive to change in temperature and atmospheric pressure. This error was effectively eliminated by the use of an atmospheric correction factor, ρ, to correct the detector reading from experimental conditions to standard conditions of temperature and pressure. This was calculated as follows:

$$\rho = \frac{P_1 T_2}{T_1 P_2}\,, \qquad (2.2)$$

where

P_1 = 760 mm of mercury, atmospheric pressure at standard conditions,

T_1 = 273° Kelvin, temperature at standard conditions,

P_2 = pressure at experimental conditions in millimeters of mercury, and

T_2 = temperature at experimental conditions in degrees Kelvin.

Leakage of the charge from the ionization chambers will occur as a result of background radiation and, in some instances, because of dirt on the insulator. Normally this leakage is not large, and for exposures of 1 hour the effect will be approximately 1.4 percent of full scale for the 1-mR chambers and about 0.2 percent for the 10-mR chambers. Obviously, for exposure of several hours duration this effect could be significant, expecially with the 1-mR chambers. However, this effect was eliminated by establishing a leakage rate for each chamber. This leakage rate was rechecked weekly and detectors with excessive leakage rates were set aside for cleaning. The leakage value was subtracted from the detector reading in the data normalization process.

All belowground radiation measurements were made with either the 1-mR dosimeters or the 10-mR dosimeters and calibrated as described in Section 2.4. The estimated error, σ_2, in the calibration of the 1-mR and 10-mR chambers against the secondary standard, was ±3.6 percent.

To estimate the error, σ_3, that may occur in the experiment as a result of different persons reading the charger reader, a test was conducted during which seventy measurements were read at various positions on the scale by nine people. The resultant standard deviation indicated a maximum error of ±1.4 percent.

Since the systematic errors of temperature, pressure, and leakage have been either eliminated or corrected, the remaining contributors to the errors of a single measurement are the source calibration error, the detector calibration error, and possible errors caused by different persons reading the minometer. The total error for a given measurement, σ_T, is calculated as follows:

$$\sigma_T = \sqrt{\sigma_1^2 + \sigma_2^2 + \sigma_3^2} = \sqrt{2^2 + 3.6^2 + 1.4^2} = 4.4\% \qquad (2.3)$$

The total experimental measurement at a given detector position consisted of the sum of four separate semiannular measurements. Since repetitive exposure-rate measurements were made for each semiannular area,

there was also a standard deviation from the mean of each semiannulus. In most cases the error was small (1 percent in semiannulus 1 for detector location C at the detector position 1 foot above the basement floor), although, in some instances for the same detector position, the standard deviation was as large as 7 percent, as in semiannulus 3. Since each semiannulus contributes only a certain percent to the total exposure, the effect of a large error in any single semiannulus would depend upon the percent contribution to the total exposure rate of that semiannulus. For example, the standard deviation for semiannulus 3 at detector position C-1 is 7 percent; however, the percent error for the sum of four semiannuli is 4.5 percent.

The total error of the measurements would be a total of the variance from systematic errors connected with the detector measurement, σ_s^2, plus the variance due to difference in the total measurements, σ_t^2 or

$$\sigma \text{ total} = \sqrt{\sigma_s^2 + \sigma_t^2} \tag{2.4}$$

The maximum total error expected at any detector position would not exceed 6.3 percent.

3. RESULTS

3.1 Free-Field Exposure Rates.

Table 3.1 shows the results of the free-field measurements. The table shows the cumulative exposure rate as a function of radius of the field in 1-foot intervals for heights of 1 to 15 feet. The exposure rates listed in Table 3.1 have been converted from semiannular to annular by multiplying by a factor of two.

According to free-field experiments reported in NDL-TR-2 (Reference 1), the exposure measurements at 3 feet above the center of a simulated fallout field of 600-foot radius constituted approximately 95 percent of the infinite-field exposure rate. For calculations necessary to determine the shielding effectiveness of structures, however, the infinite-field exposure rate is required. Since it is clearly impractical to measure the exposure rates to infinity, the free-field contribution was estimated analytically as shown in Section 4.1. The cumulative free-field exposure rates for an infinite field are shown in the last column in Table 3.1.

3.2 Open-Basement Exposure Rates.

The exposure rates measured in the open basement are shown in Table 3.2. The exposure rates are listed according to detector location (A, B, C, etc.) and to height above the basement floor. The contribution

for each annulus is listed along with the far-field contribution and the total exposure rate at each dosimeter position. The method used to determine the far-field exposure rates is explained in Section 4.2.

TABLE 3.1 CUMULATIVE FREE-FIELD EXPOSURE RATES ABOVE A RADIATION AREA AS A FUNCTION OF RADIUS AND HEIGHT

Note: Data normalized to R/h at a source density of 1 Ci/ft^2.

Detector Height Above Ground	Exposure Rates For A Radiation Area With a Radius of				Infinite* Field Exposure Rate
	60 ft	200 ft	450 ft	600 ft	
ft		R/h			R/h
1	370	463	496	502	548
2	320	419	464	472	500
3	285	388	438	447	468
4	260	366	417	428	444
5	239	343	397	409	424
6	220	324	377	387	403
7	206	310	365	377	391
8	206	313	369	382	387
9	190	288	343	357	369
10	178	276	331	344	357
11	169	263	324	337	349
12	161	258	316	330	341
13	153	249	308	322	333
14	146	244	300	313	325
15	136	235	292	306	318

*Far-field contribution beyond 600 feet was calculated - See Section 4.1.

TABLE 3.2 EXPOSURE RATES TO DETECTORS AT VARIOUS LOCATIONS IN AN OPEN CONCRETE BASEMENT LOCATED IN A RESIDUAL RADIATION AREA SIMULATED BY COBALT 60

Note: Exposure rates are in (mR/h)/(Ci/ft²).
For detector locations, see Figure 2.5.

Detector Height Above Floor (ft)	Exposure Rates for Annulus				Far-Field Exposure Rate	Total Exposure Rate
	1	2	3	4		
			Detector Location-A			
1	666	1560	2120	842	1970	7160
2	781	1650	2320	995	2330	8080
3	826	2000	2560	1080	2530	9100
4	1010	2410	3090	1280	3000	10800
5	1320	3120	4240	1590	3720	14000
6	2340	4750	5850	2270	5310	20500
			Detector Location-B			
1	880	2000	2670	1020*	2390	8960
2	1050	2230	2920	1290	3020	10500
3	1240	2790	3390	1510	3530	12500
4	1450	3480	4320	1870	4380	15500
5	1960	4490	5450	2320	5430	19700
6	3360	6560	8020	3160	7390	28500
			Detector Location-C			
1	950	2060	2860	1210	2830	9910
2	1090	2460	3200	1380	3230	11400
3	1320	2920	3560	1640	3840	13300
4	1560	3860	4480	1950	4560	16400
5	2000	5140	5680	2500	5850	21200
6	3900	6960	8380	3260	7630	30100

See footnote at end of table.

TABLE 3.2 CONTINUED

Detector Height Above Floor (ft)	Exposure Rates for Annulus				Far-Field Exposure Rate	Total Exposure Rate
	1	2	3	4		
			Detector Location-D			
1	754	1720	2400	992	2320	8180
2	920	1900	2480	1130	2640	9070
3	992	2240	2940	1250	2930	10400
4	1170	2800	3520	1550	3630	12700
5	1700	3740	5120	1910	4470	16900
6	2820	5520	6840	2680	6270	24100
			Detector Location-E			
1	864	1940	2610	1040	2430	8880
2	976	2160	2850	1250	2930	10200
3	1160	2660	3330	1440	3370	12000
4	1310	3270	4030	1700	3980	14300
5	1750	4220	5310	2150	5030	18500
6	3700	5520	6480	2780	6510	25000

*Based on Estimated Value.

3.3 Reduction Factors, Experimental and Theoretical.

The reduction factor, R, is defined as the ratio of the shielded exposure rate, D, to the free-field exposure rate at a 3-foot height above an infinitely contaminated field, D_0, i.e.,

$$R = D/D_0 \tag{3.1}$$

The experimentally determined value for the free-field exposure rate at the 3-foot height, D_0, is 468 (R/h)/(Ci/ft^2), Table 3.1. Therefore, the experimentally determined reduction factors, R_E, as shown in Table 3.3, were calculated by Equation 3.1 with the measured exposure rate at a given detector position and the experimentally determined D_0.

The theoretical reduction factors, R_T, were calculated by Spencer's method, as explained in Section 4.3.

TABLE 3.3 EXPERIMENTAL AND THEORETICAL REDUCTION FACTORS IN AN OPEN BASEMENT

Detector Height Above Floor	Location A		Location B		Location C		Location D		Location E	
	Exp.	Theo.	Exp.	Theo.	Exp.	Theo.	Exp.	Theo.	Exp.	Theo.
ft										
1	0.015	0.0079	0.019	0.015	0.021	0.018	0.017	0.010	0.019	0.013
2	0.017	0.0092	0.022	0.019	0.024	0.022	0.019	0.012	0.022	0.016
3	0.019	0.011	0.027	0.024	0.028	0.028	0.022	0.016	0.026	0.019
4	0.023	0.014	0.033	0.032	0.035	0.038	0.027	0.020	0.031	0.024
5	0.030	0.019	0.042	0.044	0.047	0.051	0.036	0.028	0.040	0.031
6	0.044	0.032	0.061	0.066	0.064	0.072	0.051	0.045	0.053	0.047

4. DISCUSSION

4.1 Estimate of Far-Field Exposure Rate Aboveground.

The exposure rate at height h along the centerline of a uniformly contaminated annulus, Figure 4.1, is given by

$$D(h;\rho_1,\rho_o) = D_1 \int_0^{2\pi} d\varphi \int_{r_1}^{r_o} B(h,\rho)\, \frac{e^{-\mu\rho}}{\rho^2}\, r dr$$

$$= 2\pi D_1 \int_{\rho_1}^{\rho_o} B(h,\rho)\, \frac{e^{-\mu\rho}}{\rho}\, d\rho\ , \qquad (4.1)$$

where

D_1 = source strength expressed as exposure rate at unit distance from a unit area of source distributed at unit density. For cobalt 60, this value is 14.3 (R/h)/(Ci/ft^2),

$B(h,\rho)$ = buildup factor at detector height, h,

$\rho_1 = \sqrt{r_1^2 + h^2}$ slant radius from the detector to the inner circle of radius r_1 of the annulus,

$\rho_o = \sqrt{r_o^2 + h^2}$ slant radius from the detector to the outer circle of radius r_o of the annulus, and

μ = total linear absorption coefficient of air for the source radiation.

It is assumed that $B(h,\rho)$ is independent of h and linear in ρ; i.e.,

$$B(\rho) = \alpha + \beta\, \mu\rho\ , \qquad (4.2)$$

where α and β are constants. Then (4.1) becomes

$$D(h;\rho_1,\rho_o) = 2\pi D_1 \left\{\alpha \left[E_1(\mu\rho_1) - E_1(\mu\rho_o)\right] + \beta \left[e^{-\mu\rho_1} - e^{-\mu\rho_o}\right]\right\}, \qquad (4.3)$$

where $E_1(x)$ denotes the exponential integral,

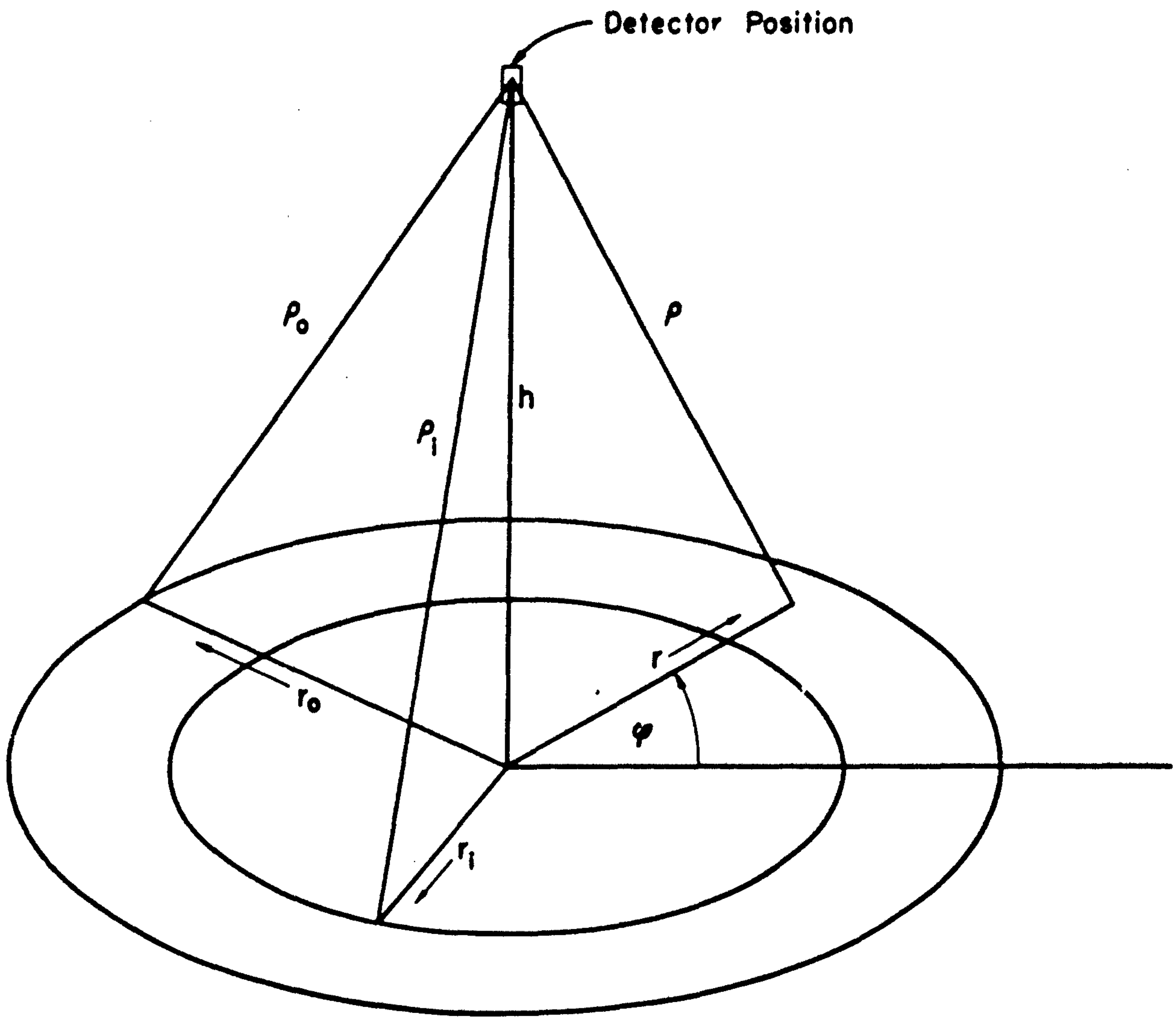

Figure 4.1 Annulus - Detector Geometry.

$$E_1(x) = \int_x^\infty \frac{e^{-t}}{t} dt \quad . \tag{4.4}$$

If α, β, and μ are specified in (4.3), theoretical exposure rates for various detector positions and annuli can readily be calculated by means of tables.

The exposure rate, $D(h;\rho_1,\infty)$, is called the theoretical far-field contribution of the exposure rate at height h. The particular case h=3, i.e., the theoretical far-field contribution of the exposure rate for the standard position, is especially important. For every ρ_1

$$D(h;h,\infty) = D(h;h,\rho_1) + D(h;\rho_1,\infty) \quad . \tag{4.5}$$

In an experiment covering a slant range, ρ_1, it is necessary to obtain an estimate for the experimental far-field contribution $D_m(h;\rho_1,\infty)$, the subscript m standing for measured.

In the experimental analogue of (4.5),

$$D_m(h;h,\infty) = D_m(h;h,\rho_1) + D_m(h;\rho_1,\infty) \quad . \tag{4.6}$$

Only $D_m(h;h,\rho_1)$ is known and all respective quantities in (4.6) are smaller than in (4.5) because of such factors as ground roughness, deviation of the field from a smooth plane, etc. The fact that

$$D_m(h,\rho_1) < D_m(h,\infty) < D(h,\infty) \quad , \tag{4.7}$$

suggests to approximate $D_m(h,\infty)$ by a weighted mean

$$M = \frac{\lambda_1 D_m(h,\rho_1) + \lambda_2 D(h,\infty)}{\lambda_1 + \lambda_2} \quad . \tag{4.8}$$

The weight of the experimental value $D_m(h,\rho_1)$ is favored over $D(h,\infty)$ because the computation of $D(h,\infty)$ assumes the validity of a buildup factor for unrestricted slant ranges. In (4.7) and (4.8) the first argument, h, denoting the detector position, has been omitted. Thus, $D_m(h,\rho_1) = D_m(h;h,\rho_1)$ and similarly for the other quantities.

If one chooses $\lambda_1 = D(h,\rho_1)$ and $\lambda_2 = D_m(h,\rho_1)$, $D_m(h,\infty)$ is approximated by

$$D_m^*(h,\infty) = D_m(h,\rho_1) \frac{D(h,\rho_1) + D(h,\infty)}{D(h,\rho_1) + D_m(h,\rho_1)} \quad . \tag{4.9}$$

Then the relative error of $D_s(h,\infty)$ is given by

$$\frac{|D_s(h,\infty) - D_s^*(h,\infty)|}{D_s(h,\infty)} = \frac{1}{D_s(h,\infty)} \left| D_s(h,\rho_1)\ \gamma - D_s(\rho_1,\infty) \right| \quad , \tag{4.10}$$

where

$$\gamma = \frac{D(h,\infty) - D_s(h,\rho_1)}{D(h,\rho_1) + D_s(h,\rho_1)} \quad . \tag{4.11}$$

Since $2\ D_s(h,\rho_1) > D_s(\rho_1,\infty)$,

$$\left| \frac{D_s(h,\infty) - D_s^*(h,\infty)}{D_s(h,\infty)} \right| < \gamma \quad , \quad \text{and} \tag{4.12}$$

one obtains the following result: For experiments such that the measured contribution from the finite part of the field exceeds 50 percent of the far-field contribution, the total exposure rate $D_s(h,\infty)$ can be approximated by $D_s^*(h,\infty)$ with a relative error considerably less than γ.

The mild condition stated is always satisfied in elaborate experiments. That the relative error is in fact considerably less than γ follows from the details of removing the unknowns $D_s(\rho_1,\infty)$ and $D_s(h,\infty)$ from the right side of (4.10). From Reference 1 the values $\alpha = 1.11$, $\beta = 0.529$ are used; i.e.,

$$B(\rho) = 1.11 + 0.529\ \mu\rho \quad . \tag{4.13}$$

One obtains with $\mu = 2.24 \cdot 10^{-3}$ ft $^{-1}$, $\rho_1 = 600$ ft, for the standard position $h = 3$ from (4.3), (4.9), and (4.11),

$$D_s(3;3,\infty) \approx D_s^*(3;3,\infty) = 468 \text{ R/h} \tag{4.14}$$

with % Error $\left[D_s(3;3,\infty)\right] < 5\%$. As shown in Reference 1, the buildup factor (4.13) is valid for slant ranges up to 800 feet. It is assumed that its use for unrestricted slant ranges introduces only negligible error. Similarly, it is expected that all constants in the pertinent equations do not change appreciably up to heights of 15 feet (Reference 10). Far-field corrections for other heights have accordingly been made, as shown above for the standard position.

4.2 Experimental Exposure Rates in Basement.

If in (4.1) β is replaced by $(\beta-1)$, the exposure rate $D^{(s)}(h;\rho_1,\rho_0) \equiv D^{(s)}(\rho_1,\rho_0)$ due to skyshine only is obtained. $D^{(s)}(\rho_1,\rho_0)$ also represents the theoretical skyshine contribution in an open structure below ground.

From (4.3) it follows that

$$(2\pi D_1)^{-1} D^{(s)}(\rho_1,\rho_0) = (\alpha-1)\left[E_1(\mu\rho_1) - E_1(\mu\rho_0)\right] + \beta\left[e^{-\mu\rho_1} - e^{-\mu\rho_0}\right] . \quad (4.15)$$

With the method below, an estimate for the experimental far-field contribution $D_m^{(s)}(\rho_1,\infty)$ is obtained. Since

$$(2\pi D_1)^{-1} D^{(s)}(h,\infty) = (\alpha-1)E_1(\mu h) + \beta e^{-\mu h} ,$$

$$(2\pi D_1)^{-1} D^{(s)}(h,\rho_0) = (\alpha-1)\left[E_1(\mu h) - E_1(\mu\rho_0)\right] + \beta\left[e^{-\mu h} - e^{-\mu\rho_0}\right] , \text{ and}$$

$$(2\pi D_1)^{-1} D^{(s)}(\rho_0,\infty) = (\alpha-1)E_1(\mu\rho_0) + \beta e^{-\mu\rho_0} ,$$

$$D^{(s)}(h,\infty) = D^{(s)}(h,\rho_0) + C(\rho_1,\rho_0)\, D^{(s)}(\rho_1,\rho_0) , \quad (4.16)$$

where

$$C(\rho_1,\rho_0) = \frac{(\alpha-1)\, E_1(\mu\rho_0) + \beta e^{-\mu\rho_0}}{(\alpha-1)\left[E_1(\mu\rho_1) - E_1(\mu\rho_0)\right] + \beta\left[e^{-\mu\rho_1} - e^{-\mu\rho_0}\right]} . \quad (4.17)$$

In (4.16) the theoretical far-field contribution is represented as the product of the ring contribution $D^{(s)}(\rho_1,\rho_0)$ and the correction factor $C(\rho_1,\rho_0)$. It is assumed now that the corr[illegible]on factor $C(\rho_1,\rho_0)$ can be applied to the experimental value $D_m^{(s)}(\rho_1,\rho_0)$; tha[illegible] for the experimental case

$$D_m^{(s)}(h,\infty) \approx D_m^{(s)}(h,\rho_0) + C(\rho_1,\rho_0)\, D_m^{(s)}(\rho_1,\rho_0) , \quad (4.18)$$

where $D_m^{(s)}(\rho_1,\rho_0)$, the contribution from the outermost annulus, is taken since it is expected that skyshine contributions from the far field and the last annulus behave similarly. Although the method is widely adopted, it is difficult to find an error estimate in terms of readily computed quantities. None has been offered so far. Because of the differences in the denominator of (4.17), the small value of μ, and the behavior of $E_1(x)$, the method should never be applied to small outer annuli. An attempt to adapt the method of (4.1) to the present skyshine case is not very promising. Since the far-field contribution can easily amount to 30 to 40 percent of the contribution from the finite part of the field even in elaborate experiments, it is difficult to find close lower and upper bounds for $D_m^{(s)}(h,\infty)$ that allow a general error estimate of practical value.

The far-field exposure rates presented in Table 3.2 were obtained by the above method applied to the fourth annulus.

4.3 Reduction Factors.

The various detector positions in the basement at which measurements were taken, along with the solid angle fractions subtended at them by the rectangular opening of the basement, are listed in Table 4.1. A rectangular coordinate system centered at the middle of the basement floor with the positive x-direction CD, positive y-direction CE, and positive h-direction pointing towards the opening has been introduced. The ω-values were calculated as outlined in Section 41 of NBS 42 (Reference 4).

TABLE 4.1 DETECTOR POSITIONS WITH CORRESPONDING SOLID-ANGLE FRACTIONS

ω \ h	1	2	3	4	5	6
A(9,4,h)	0.197	0.224	0.259	0.308	0.389	0.563
B(4.5,2,h)	0.326	0.386	0.461	0.556	0.677	0.828
C(0,0,h)	0.370	0.436	0.516	0.614	0.729	0.859
D(9,0,h)	0.243	0.284	0.337	0.409	0.511	0.679
E(0,4,h)	0.298	0.342	0.395	0.461	0.551	0.701

Theoretically, detector positions with equal ω-values should yield similar exposure rates. A comparison of exposure rates measured at detector positions with nearly equal ω-values shows that they are appreciably influenced by radiation backscattering from the floor and walls. It is not possible to dispose of the backscattering component with a flat percentage (20 percent or so). It would appear, therefore, that inaccuracies will result from using a single factor (1.2) to account for the backscattering component in a concrete basement. A clear separation of the skyshine component from the backscattering component calls for future experimentation, possibly with leaded and unleaded walls.

Ideally, theoretical reduction factors, R, should take the following form:

$$R = \frac{D}{D_o} = \frac{D}{D(3;3,\infty)} = f(h,\omega)\ S_a(d = 0,\omega) \qquad (4.19)$$

where the function $S_a(d = 0,\omega)$ is the geometry function defined by formula (27.13) of NBS 42, and $f(h,\omega)$ is the position function. The position function includes the skyshine detector response at ground level $S(d = 0)$ and the response to radiation backscattered from the side walls and floor, which is a function of height, h, above the basement floor and the solid-angle fraction, ω, subtended at the detector. However, the only theoretical formulation available for calculating reduction factors for a case which resembles closely the open-basement situation is the approximate skyshine response formula for a foxhole [formula (31.1), NBS 42]

$$\frac{D}{D_0} = 1.2\ S(d = 0)\ S_a(d = 0,\omega)\ . \tag{4.20}$$

Reduction factors computed from (4.20) are listed in Table 3.3, along with those found experimentally at corresponding detector positions A through E. At positions along the centerline, relatively good agreement is observed. Note that the theoretical and experimental reduction factors are not directly comparable since the far-field correction factor $C(\rho_1,\rho_0)$ should be applied only to the skyshine contribution and not to the sum of the skyshine and backscattering component.

Figure 4.2 describes the nature of the experimental position function $f(h,\omega)$ for the open basement. This figure shows the experimental position function $f\ (h,\omega)$ plotted against the solid-angle fraction, ω, for detector height, h, where R is the experimental reduction factor. The detector location for each point of the height curves may be found by matching the points with the solid-angle fractions shown in Table 4.1. For comparison the corresponding theoretical representation (4.20) is included and is described by the line $1.2\ S(d = 0)$, parallel to the ω-axis.

Figure 4.2 shows that, in a concrete basement, detector response to skyshine radiation depends upon position in the basement and height above the floor. Indications are that in a rectangular basement the theoretical calculation as given in Equation (4.20) will only approximate the center or near-center detector locations but is not good for eccentric off-center detector locations. According to Equation (4.20) the quantity $1.2\ S(d = 0)$ should be constant for all solid angles. Figure 4.2 shows that this does not hold throughout the basement but varies according to horizontal and vertical positions. Since the function $S(d = 0)$, which describes the amount of skyshine radiation entering the basement at ground level, should not vary according to detector location, then the difference would be caused by the inaccurate estimation of the contribution due to backscattering from the side walls and the floor, or the 1.2 factor. For any detector position in the basement an approximate reduction factor can be interpolated by means of Figure 4.2.

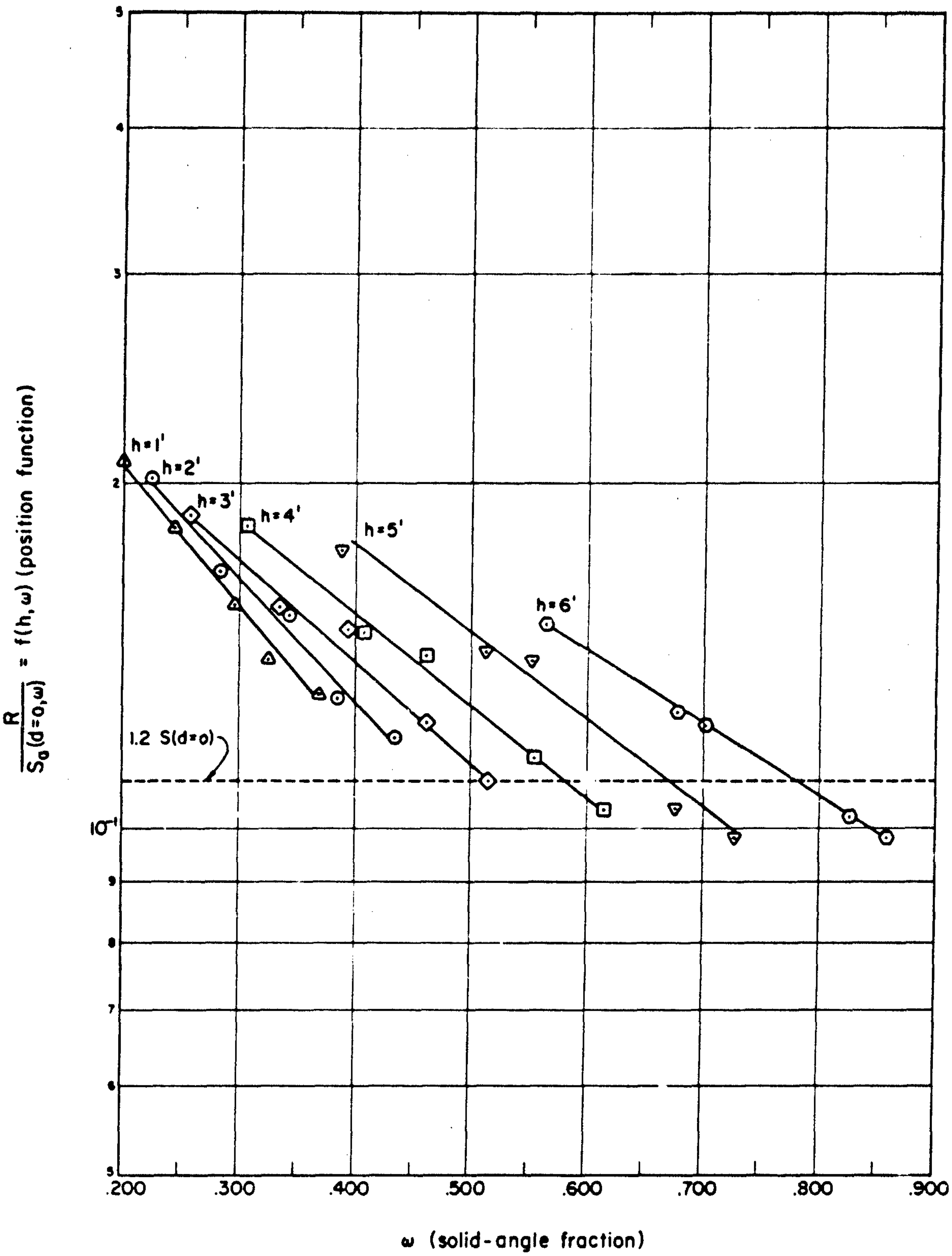

Figure 4.2 Graph showing the experimental position function $f(h,\omega) = \frac{R}{S_a(d = 0,\omega)}$ versus the solid-angle fraction, ω, for various heights above the basement floor.

4.4 Comparison of Experimental and Theoretical Reduction Factors.

The difference between experimental and theoretical reduction factors at various detector locations and positions within a concrete basement are shown in Table 4.2 and plotted in Figures 4.3 through 4.7.

TABLE 4.2 COMPARISON OF EXPERIMENTAL AND THEORETICAL REDUCTION FACTORS

Detector Height Above Floor	Percent Differences at Detector Locations*				
	A	B	C	D	E
ft			percent		
1	47	21	14	41	32
2	46	14	8	37	27
3	42	11	0	27	27
4	39	3	-9	26	23
5	37	-5	-8.5	22	23
6	27	-8	-13	12	11

$$\text{*Percent Difference} = \frac{\text{Experimental-Theoretical}}{\text{Experimental}} \times 100$$

The largest range of differences is seen at all heights of detector location A, Figure 4.3. For all heights at this detector location, the experimental values ranged from 27 to 47 percent higher than the theoretical values. These rather large differences are due in part to the error caused by using a single correction for backscattered radiation and partly to the fact that the detector location A is in a highly eccentric position with respect to the overhead opening. The theoretical calculations are best suited for a detector location in the center of the basement. Spencer states that calculated results under highly eccentric geometries (i.e., the value of the length-to-width ratio, e, greater than 3) would greatly underestimate the experimental results (Reference 4).

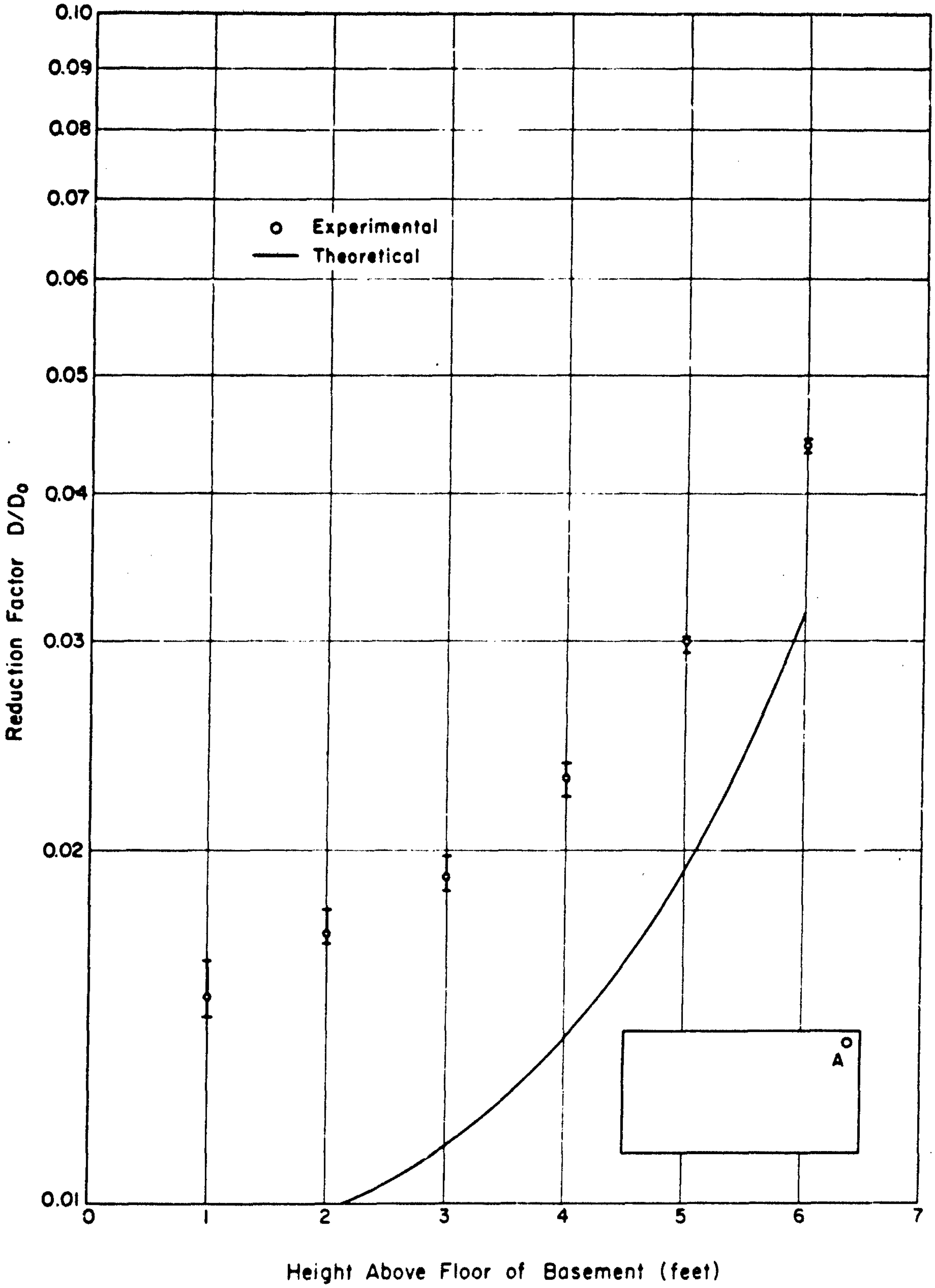

Figure 4.3 Experimental and theoretical reduction factors versus height above an open basement floor, detector location A.

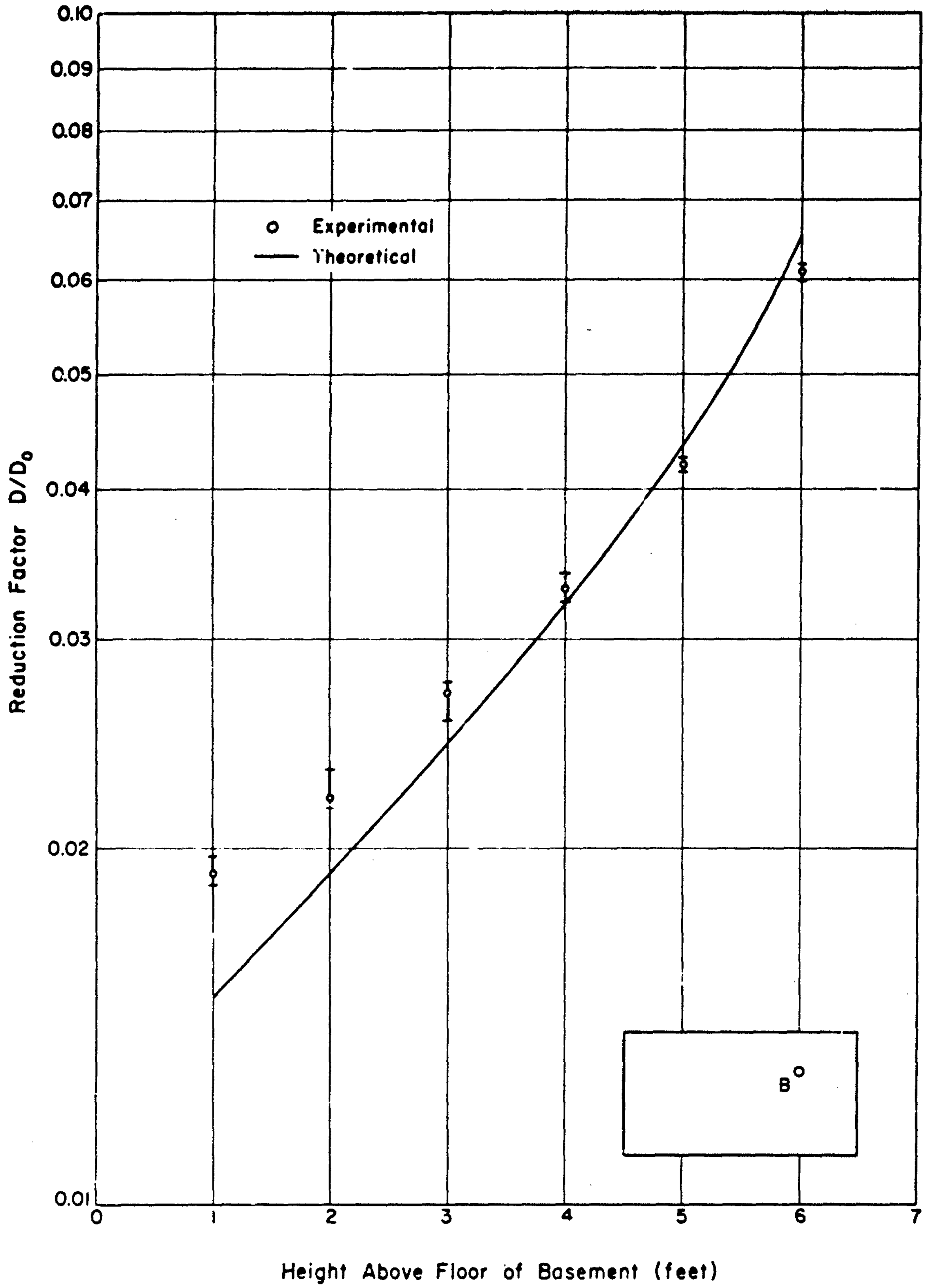

Figure 4.4 Experimental and theoretical reduction factors versus height above an open basement floor, detector location B.

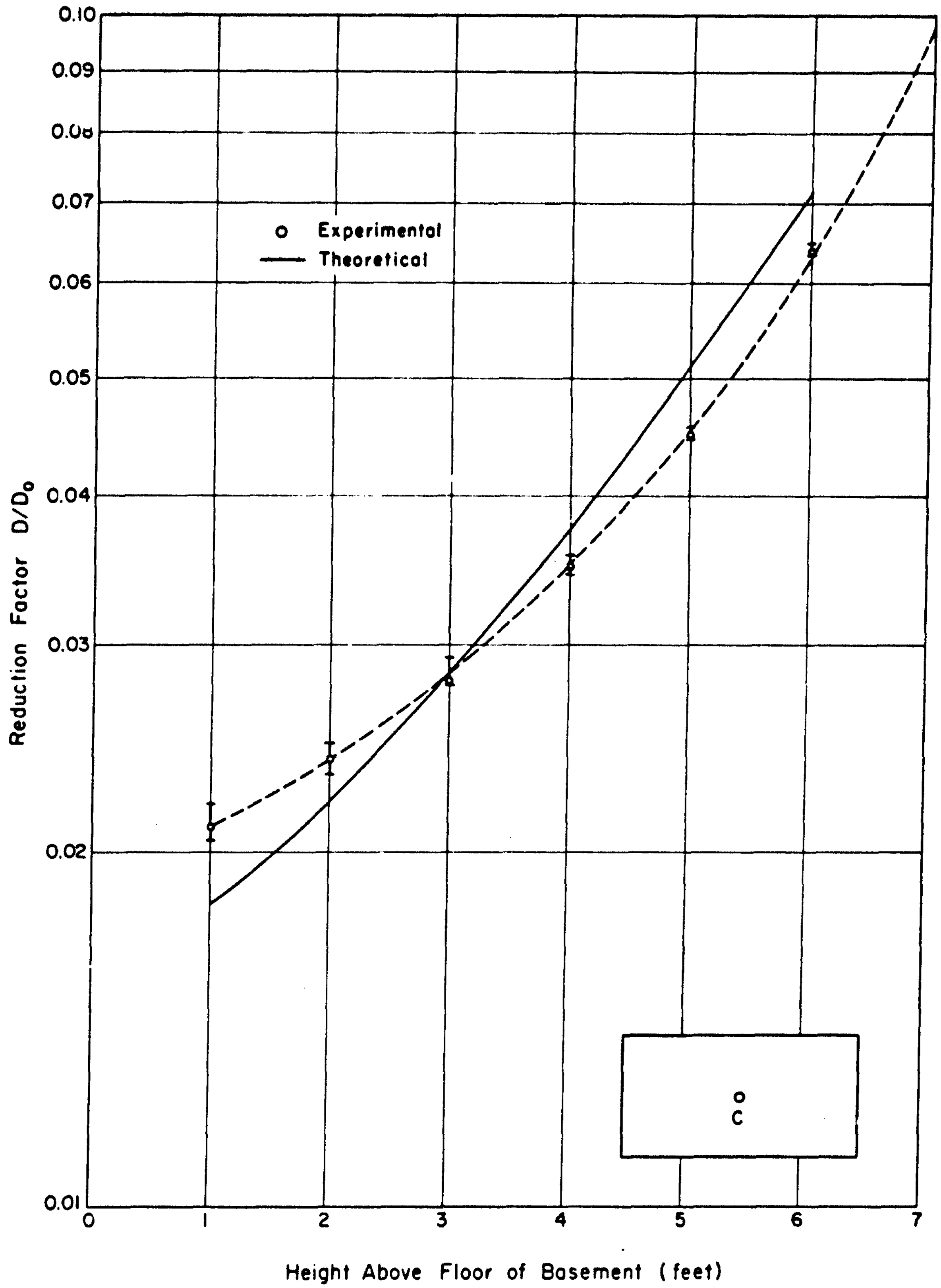

Figure 4.5 Experimental and theoretical reduction factors versus height above an open basement floor, detector location C.

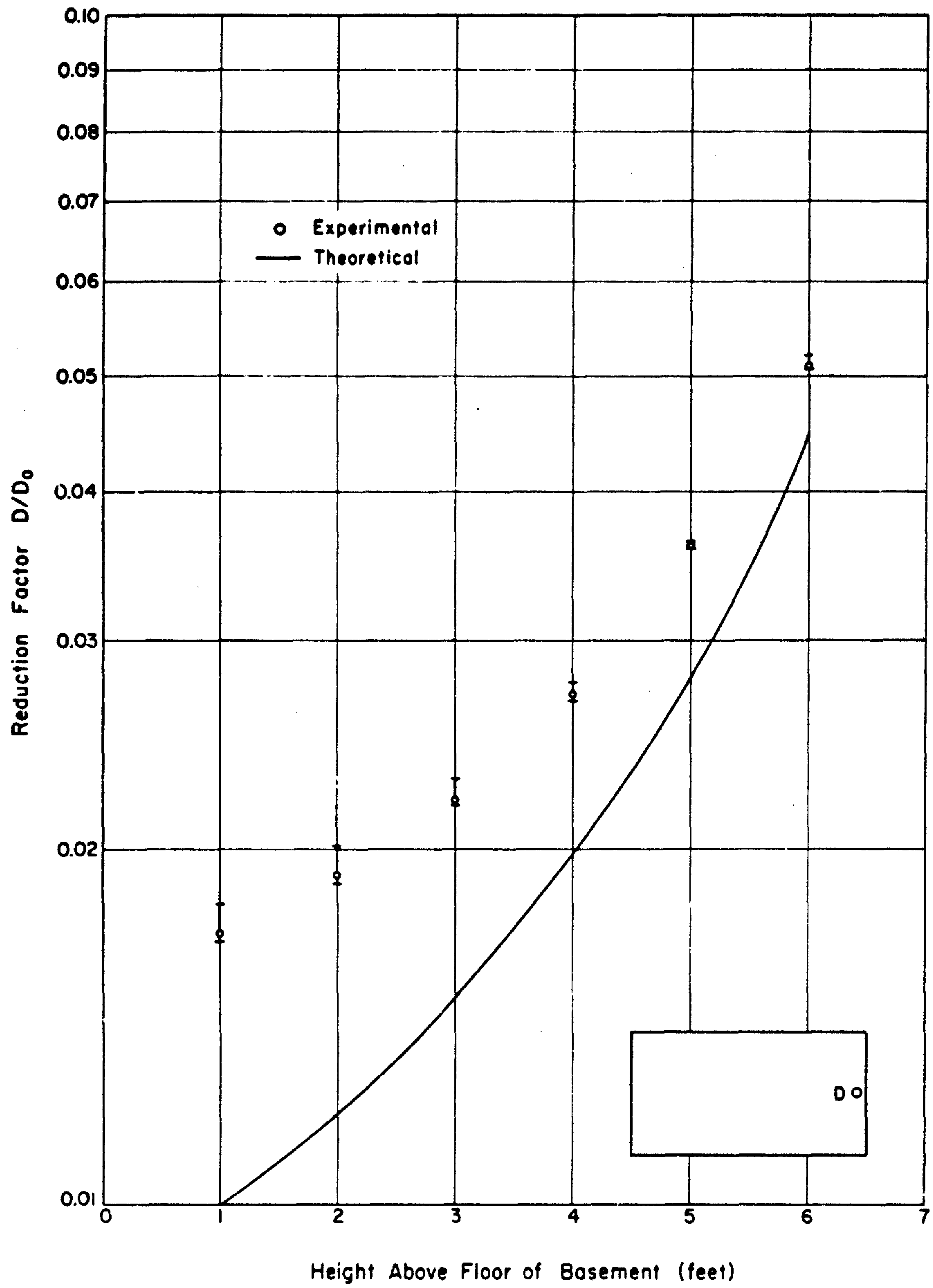

Figure 4.6 Experimental and theoretical reduction factors versus height above an open basement floor, detector location D.

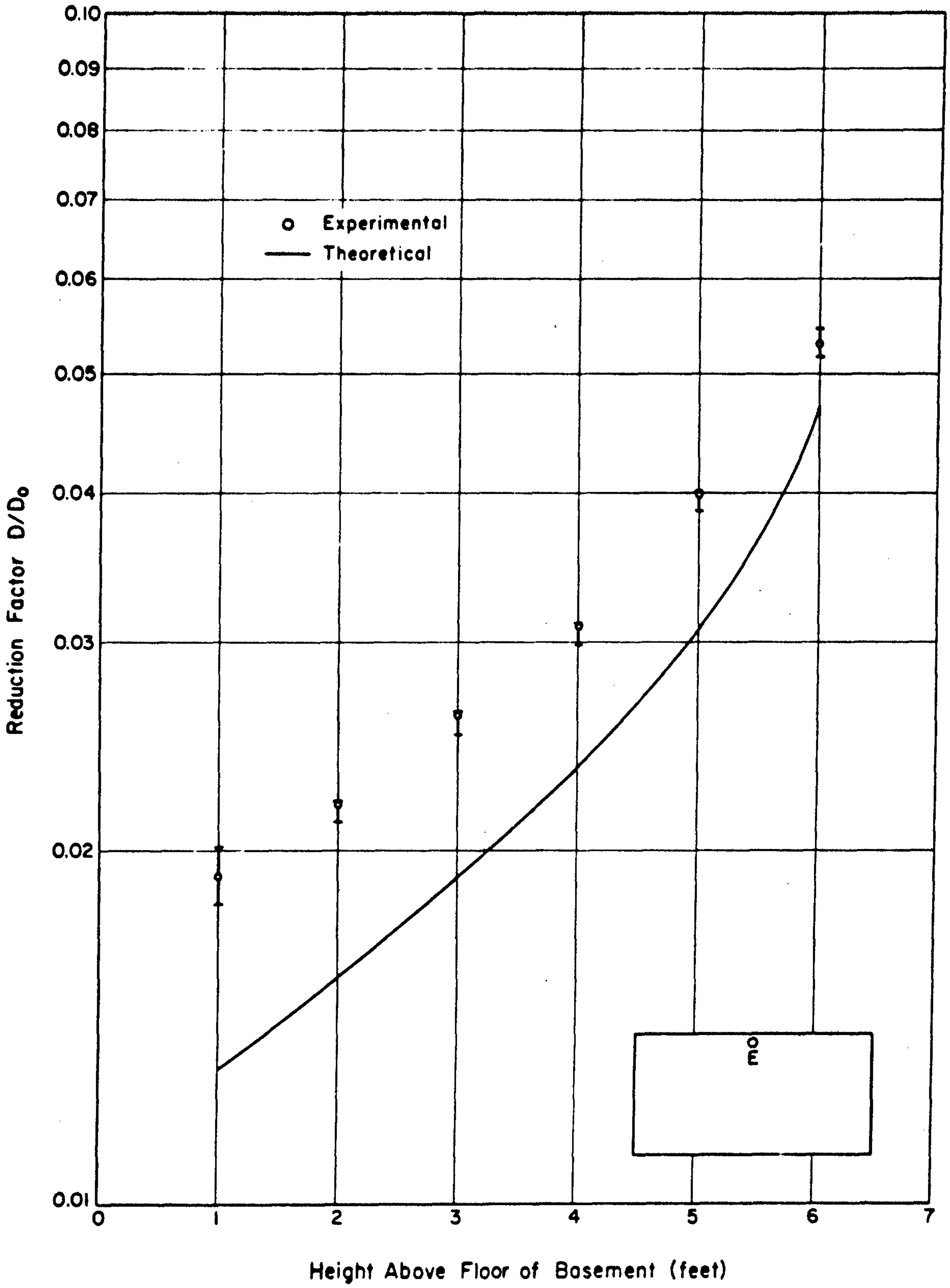

Figure 4.7 Experimental and theoretical reduction factors versus height above an open basement floor, detector location E.

A similar explanation pertaining to eccentric detector geometries can be made for the differences in experiment and theory at detector location D, Figure 4.6, although the difference is not as large as that at detector location A. The reason for this was that detector location D was oriented along the centerline of the width of the basement and was less eccentric than detector location A.

Note that the larger percent differences (Table 4.2) between experiment and theory, probably due to backscattered radiation, occur at all detector positions next to the walls and floor, e.g., corner detector location A, and wall detector locations D and E. The radiation backscatter contribution is emphasized in comparing the percent differences for detector locations A, D, and E. Here, the percent differences between experiment and theory are largest for those detector positions that are next to the larger wall-surface areas.

Agreement between experimental and theoretical reduction factors was good at detector locations B and C, Figures 4.4 and 4.5. This would be expected at the C detectors located at the center of the basement. However, in view of the results from the other detector locations (A, D, and E), the close agreement at detector location B is somewhat surprising. Again, the explanation appears to be that detector location B, although off-center, was somewhat nearer the center than the other detector locations.

It was noted that, at all detector locations, the agreement between experiment and theory was best at the detector positions near the top of the basement. In Figures 4.3 through 4.7, the experimental data taken near the basement floor curves upward, whereas the theoretical curve continues to fall off approximately exponentially. This again indicates that in a large open basement there may be the additional buildup of radiation due to backscatter from the floor that is not accounted for with the 1.2 factor recommended in NBS Monograph 42.

Figure 4.5 shows the exposure rate plotted versus the height above the basement floor at the center detector location. The experimental curve was extrapolated to the 7-foot height (ground level) or ω=1. The extrapolated value 0.0987, from Figure 4.5, times the free-field exposure rate, 468,000 (mR/h)/(Ci/ft^2) at the 3-foot height, yields an exposure rate of 46,500 (mR/h)/(Ci/ft^2) at ground level. This value, of course, would include any backscatter from the walls and the floor. If a backscatter of 20 percent is assumed and subtracted, then the total exposure rate due to skyshine at the surface of the basement would be 37,200 (mR/h)/(Ci/ft^2). This is 7.9 percent of the infinite free-field exposure rate at the 3-foot height above ground. This compares favorably with 8.8 percent calculated by Spencer (Reference 4) and 10 percent measured by Burson and Summers (Reference 8).

5. CONCLUSIONS

Analysis of the position function f(h,ω) at various detector levels above the basement floor indicates the presence of a backscattering contribution that is dependent on height above the floor and solid-angle fraction and is not adequately estimated by a single correction factor (1.2 suggested in NBS Monograph 42).

Agreement within 21 percent was obtained between experimental and theoretical reduction factors calculated by Formula (31.1) of NBS Monograph 42 for detector locations in the center or near the center of the basement (detector locations C and B).

Theoretical reduction factors underestimate experimental reduction factors at the off-center detector locations close to the basement wall (detector locations A, D, and E) by as much as 47 percent. The differences appear to be caused by radiation scattered from the walls and floor of the basement; this scattering is not completely accounted for in the theoretical calculations.

Extrapolation to the ground surface (ω = 1) of the experimentally measured reduction factors at the center detector location within the open concrete basement yields an exposure rate that is 7.9 percent of the infinite free-field exposure rate at the 3-foot height. This compares favorably with 8.8 percent calculated in the NBS Monograph 42.

The infinite-field exposure rate at the 3-foot height above a graded, rolled, and relatively smooth field was measured as 468 R/h at a source density of 1 Ci/ft^2 of cobalt-60 radiation simulated with a circulating point source.

LITERATURE CITED

1. Rexroad, R. E. and Schmoke, M. A.; Scattered Radiation and Free-Field Dose Rates from Distributed Cobalt 60 and Cesium 137 Sources; NDL-TR-2, September 1960; US Army Chemical Corps Nuclear Defense Laboratory, Army Chemical Center, Maryland; Unclassified.

2. Schmoke, M. A., and Rexroad, R. E.; Attenuation of Simulated Fallout Radiation by the Roof of a Concrete Blockhouse; NDL-TR-6, August 1961; US Army Chemical Corps Nuclear Defense Laboratory, Army Chemical Center, Maryland; Unclassified.

3. Schmoke, M. A. and Rexroad, R. E.; Attenuation of Fallout Radiation as a Function of Concrete Blockhouse Wall Thickness; NDL-TR-43, October 1963; US Army Nuclear Defense Laboratory, Edgewood Arsenal, Maryland; Unclassified.

4. Spencer, L. V.; Structure Shielding Against Fallout Radiation from Nuclear Weapons; NBS Monograph 42, 1 June 1962; National Bureau of Standards, Washington, D.C.; Unclassified.

5. Office of Civil Defense; Design and Review of Structures for Protection from Fallout Gamma Radiation; OCD Professional Manual, Series PM-100-1, February 1965; Unclassified.

6. Clifford, C. E., Carruthers, J. A., and Cunningham, J. R.; Scattered Gamma Radiation from a Simulated Fallout Field Using Cesium-137; DRCL Report 296, January 1959; Defense Research Chemical Laboratories, Ottawa, Canada; Unclassified.

7. Starbird, A. W., and Batter, J. F.; Angular Distribution of Skyshine Radiation at the Surface of a Plane of Fallout Contamination; TO-B-63-40, March 1964; Technical Operations Research, Burlington, Massachusetts; Unclassified.

8. Burson, Z. G. and Summers, R. L.; Barrier Attenuation of Air-Scattered Gamma Radiation; CEX-63.3, December 1964; US Atomic Energy Commission, Las Vegas, Nevada; Unclassified.

9. Rexroad, R. E., Schmoke, M. A., and Schumchyk, M. J.; A Point-Source Circulation System for Simulating Fallout Gamma Radiation; NDL-TM-15, December 1964; US Army Nuclear Defense Laboratory, Edgewood Arsenal, Maryland; Unclassified.

10. McDonnell C., et.al.; Description, Experimental, Calibration and Analysis of the Radiation Test Facility at the Protective Structures Development Center; PSDC-TR-14, 1 September 1964; Protective Structures Development Center, Fort Belvoir, Virginia; Unclassified.

LITERATURE CITED (Continued)

11. Berger, M. J.; Calculation of Energy Dissipation by Gamma Radiation Near the Interface Between Two Media; Journal of Applied Physics, Volume 28, No. 12, 1502-1508; December 1957.

12. Clarke, E. T. and Batter, J.; Gamma-Ray Scattering by Nearby Surfaces, Transactions of American Nuclear Society, Volume 5, No. 1, 223; June 1962; Unclassified.

13. Eisenhauer, C.; Analysis of Experiments on Light Residual Structures with Distributed Cobalt 60 Sources; NBS 6539, October 1959; National Bureau of Standards, Washington, D.C.; Unclassified.

14. Huddleston, C. M., et.al.; Ground Roughness Effects on the Energy and Angular Distribution of Gamma Radiation from Fallout Radiation; CEX 62.81, July 1964; US Atomic Energy Commission, Las Vegas, Nevada; Unclassified.

APPENDIX A

EXPERIMENTAL DATA

Tables A.1 through A.8 contain the data for each detector position at the various locations within a concrete basement. The exposure-rate contributions are given for all four semiannuli of the radiation area with the sum of the four semiannuli shown in the column to the right.

To obtain the total exposure rate from the simulated fallout field for detectors at locations, A, B, and E, the exposure rate of the primary positions A, B, and E are added to the exposure rate of the image positions a, b, and e, respectively. At each height for detector locations C and D, the exposure rates are doubled.

TABLE A.1 EXPOSURE RATE CONTRIBUTION TO PRIMARY DETECTORS AT LOCATION (A) FROM VARIOUS SEMIANNULI OF A SIMULATED FALLOUT FIELD

Note: Exposure rates are in (mR/h)/(Ci/ft^2)

Detector Height Above Floor (ft)		Exposure Rate Contribution From Semiannulus				Σ 1 through 4
		1	2	3	4	
1		262	600	777	363	
		261	696	794	321	
			532		362	
					303	
	Average	262	609	786	337	1990
2		302	627	971	426	
		283	618	975	400	
			597		381	
					381	
					351	
	Average	293	614	973	388	2270
3		350	714	943	446	
		318	682	956	418	
			694		375	
					433	
					370	
	Average	334	697	950	408	2390
4		380	851	1110	460	
		362	862	1170	442	
		370	865		468	
			813		453	
	Average	371	848	1140	456	2820
5		467	1050	1390	535	
		483	962	1460	522	
		507	1020		528	
			1110		537	
			999			
			1060			
	Average	486	1030	1430	531	3480
6		802	1650	2100	852	
		813	1690	2170	859	
			1760		866	
	Average	808	1700	2140	859	5510

TABLE A.2 EXPOSURE RATE CONTRIBUTION TO IMAGE DETECTORS AT LOCATION (a) FROM VARIOUS SEMIANNULI OF A SIMULATED FALLOUT FIELD

Note: Exposure rates are in $(mR/h)/(Ci/ft^2)$

Detector height Above Floor (ft)		Exposure Rate Contribution From Semiannulus 1	2	3	4	Σ 1 through 4
1		434	941	1450	516	
		372	945	1200	487	
			963		512	
					504	
	Average	404	950	1330	505	3190
2		490	969	1360	596	
		485	1110	1340	617	
			1050			
	Average	488	1040	1350	607	3490
3		500	1280	1630	673	
		483	1300	1580	677	
			1260		651	
			1360			
	Average	492	1300	1610	667	4070
4		637	1590	2040	852	
		634	1550	1860	801	
			1520		814	
			1510			
			1610			
			1550			
			1590			
	Average	636	1560	1950	822	4970
5		826	2070	2810	1030	
		837	2110		1080	
			2100			
	Average	832	2090	2810	1060	6790
6		1530	3080	3710	1370	
		1530	3040		1440	
			3040			
	Average	1530	3050	3710	1410	9700

TABLE A.3 EXPOSURE RATE CONTRIBUTION TO PRIMARY DETECTORS AT LOCATION (B) FROM VARIOUS SEMIANNULI OF A SIMULATED FALLOUT FIELD

Note: Exposure rates are in (mR/h)/(Ci/ft^2)

Detector Height Above Floor (ft)		Exposure Rate Contribution From Semiannulus				Σ 1 through 4
		1	2	3	4	
1		426	899	1110		
		374	886	1100		
			902			
	Average	400	896	1110	390*	2800
2		484	919	1260	600	
		441	936	1240	648	
					547	
					520	
					573	
					600	
	Average	463	928	1250	581	3220
3		561	1220	1550	597	
		529	1140	1500	698	
			1180			
	Average	545	1180	1530	648	3900
4		652	1500	1790	772	
		649	1450	1860	806	
			1430		866	
			1550			
			1560			
	Average	651	1500	1830	815	4800
5		902	1910	2340	989	
		915	1940		1040	
		915	2050			
	Average	910	1970	2340	1010	6230
6		1710	2930	3680	1360	
		1670	2980		1480	
		1740			1420	
		1610				
	Average	1680	2960	3680	1420	9740

*Graphically interpolated.

TABLE A.4 EXPOSURE RATE CONTRIBUTION TO IMAGE DETECTORS AT LOCATION (b) FROM VARIOUS SEMIANNULI OF A SIMULATED FALLOUT FIELD

Note: Exposure rates are in (mR/h)/(Ci/ft²)

Detector Height Above Floor (ft)	Exposure Rate Contribution From Semiannulus				Σ 1 through 4
	1	2	3	4	
1	479	1090	1510	623	
		1110	1600	666	
		1090		617	
				669	
				590	
Average	479	1100	1560	633	3770
2	601	1310	1710	682	
	567	1280	1620	727	
		1300		724	
Average	584	1300	1670	711	4270
3	700	1660	1860	818	
	690	1580		891	
		1520		872	
		1690			
Average	695	1610	1860	860	5030
4	790	1910	2490	1110	
	801	1940		1000	
	805	2060		1040	
		2000			
Average	799	1980	2490	1050	6320
5	1060	2450	3110	1310	
	1020	2440		1300	
	1070	2590			
Average	1050	2520	3110	1310	7990
6	1630	3620	4340	1740	
	1670	3630		1740	
	1730	3560			
	1690				
Average	1680	3600	4340	1740	11400

TABLE A.5 EXPOSURE RATE CONTRIBUTION TO DETECTORS AT LOCATION (C) FROM VARIOUS SEMIANNULI OF A SIMULATED FALLOUT FIELD

Note: Exposure rates are in (mR/h)/(Ci/ft^2)

Detector Height Above Floor (ft)		Exposure Rate Contribution From Semiannulus				Σ 1 through 4
		1	2	3	4	
1		470 481	1060 1010 1030	1530 1410 1340	601 609 625 594	
	Average	475	1030	1430	607	3540
2		560 534	1240 1210 1230	1650 1610 1550	712 699 672 707 652	
	Average	547	1230	1600	688	4070
3		675 640	1450 1470	1800 1750	801 788 867	
	Average	658	1460	1780	819	4720
4		767 790 790	1880 1960 1940	2310 2240 2180	982 958 988	
	Average	782	1930	2240	976	5930
5		995 1010 1000	2570 2580 2560	2840	1250 1220 1270	
	Average	1000	2570	2840	1250	7660
6		1970 1930 1960 1930	3550 3410 3470	4190	1620 1650 1620	
	Average	1950	3480	4190	1630	11300

TABLE A.6 EXPOSURE RATE CONTRIBUTION TO DETECTORS AT LOCATION (D) FROM VARIOUS SEMIANNULI OF A SIMULATED FALLOUT FIELD

Note: Exposure rates are in (mR/h)/(Ci/ft^2)

Detector Height Above Floor (ft)		Exposure Rate Contribution From Semiannulus				Σ 1 through 4
		1	2	3	4	
1		380	876	1180	511	
		372	849	1220	522	
			854		459	
					506	
					481	
	Average	376	860	1200	496	2930
2		437	944	1260	577	
		483	949	1210	600	
			958		562	
					560	
					537	
	Average	460	950	1240	567	3220
3		496	1150	1480	618	
			1090	1460	609	
			1120		625	
					658	
					610	
	Average	496	1120	1470	624	3710
4		581	1430	1790	767	
		589	1380	1730	783	
			1360			
			1380			
			1390			
			1460			
	Average	585	1400	1760	775	4520
5		850	1860	2560	958	
		850	1870		953	
	Average	850	1870	2560	956	6240
6		1410	2740	3420	1300	
		1410	2770		1370	
		1410				
	Average	1410	2760	3420	1340	8930

TABLE A.7 EXPOSURE RATE CONTRIBUTION TO PRIMARY DETECTORS AT LOCATION (E) FROM VARIOUS SEMIANNULI OF A SIMULATED FALLOUT FIELD

Note: Exposure rates are in $(mR/h)/(Ci/ft^2)$

Detector Height Above Floor (ft)	Exposure Rate Contribution From Semiannulus 1	2	3	4	Σ 1 through 4
1	348	714	1080	419	
	314	779	944	435	
			852	389	
				394	
Average	331	747	959	409	2450
2	394	809	1090	494	
	358	806	1080	456	
		809	1020	486	
				485	
				468	
Average	376	808	1060	478	2720
3	424	933	1170	505	
	428	933	1220	511	
		948	1160	516	
				485	
				524	
Average	426	938	1180	508	3050
4	467	1050	1360	562	
	473	1020	1370	610	
	465	1040		564	
		1070			
Average	468	1050	1370	579	3470
5	695	1390	1810	767	
	657	1400	1740	730	
	637	1410	1680	769	
		1400			
Average	663	1400	1740	755	4560
6	2190	2010	2240	1020	
	2150	1990		1040	
	1710	2080			
	2190				
Average	2060	2030	2240	1030	7360

TABLE A.8 EXPOSURE RATE CONTRIBUTION TO IMAGE DETECTORS AT LOCATION (e) FROM VARIOUS SEMIANNULI OF A SIMULATED FALLOUT FIELD

Note: Exposure rates are in (mR/h)/(Ci/ft^2)

Detector Height Above Floor (ft)		Exposure Rate Contribution From Semiannulus				Σ 1 through 4
		1	2	3	4	
1		542	1170	1790	659	
		523	1200	1500	633	
			1210		610	
					630	
	Average	533	1190	1650	633	4010
2		618	1330	1790	784	
		582	1360	1780	783	
					745	
	Average	600	1350	1790	771	4510
3		738	1690	2200	909	
		722	1740	2100	959	
			1720			
	Average	730	1720	2150	934	5530
4		821	2230	2570	1100	
		863	2210	2750	1130	
			2210		1130	
	Average	842	2220	2660	1120	6840
5		1080	2840	3560	1410	
		1080	2810	3570	1340	
		1110	2800		1410	
	Average	1090	2820	3570	1390	8870
6		1620	3470	4190	1710	
		1650	3490	4280	1740	
		1650	3520		1810	
	Average	1640	3490	4240	1750	11100

APPENDIX B

SOURCE CALIBRATION

All circulating point sources used in the experiment were carefully calibrated to determine the radiation output (effective curie strength) of the source. In addition, to determine the validity of previous calibrations (Reference 1), all stationary point sources used in previous experimental work were recalibrated by a different geometrical arrangement.

The stationary point source and detector were supported at a height of 12.5 feet above ground. The source shield rested on a 10-foot-high platform and the detector was held in a holder fastened to a 12-foot-high ladder, Figure B.1. Exposure-rate measurements were made at horizontal source-to-detector distances of 2 feet, 4 feet, and 6.23 feet. At least 5 exposures were made at each separation distance with all measurements falling within 2 percent of the average.

To obtain an accurate estimate of the effective curie strength of the radiation source, a measurement must be made of the uncollided (narrow-beam) exposure rate at a known distance between the source and the detector. A direct measurement of this uncollided beam is complicated by the presence of air-scattered radiation and in some instances ground-scattered radiation. Therefore, the contribution from these two effects must be either eliminated or accurately estimated. The air-scattered component was estimated by using the infinite air-medium buildup factor $B(\mu r)$ of Berger (Reference 11) The air-ground interface buildup factor, as measured by Batter and Clark (Reference 12), was used to account for ground-scattered radiation.

The corrected exposure rate at 1 foot was obtained by the following formula:

$$D_1 = D_x \frac{x^2}{B(\mu x) K e^{-\mu x}} , \qquad (B.1)$$

where

D_1 = corrected exposure rate at 1 foot, R/h,

D_x = measured exposure rate at standard atmospheric conditions, R/h,

x = distance from source to detector, feet,

$B(\mu x)$ = infinite air-medium buildup factor,

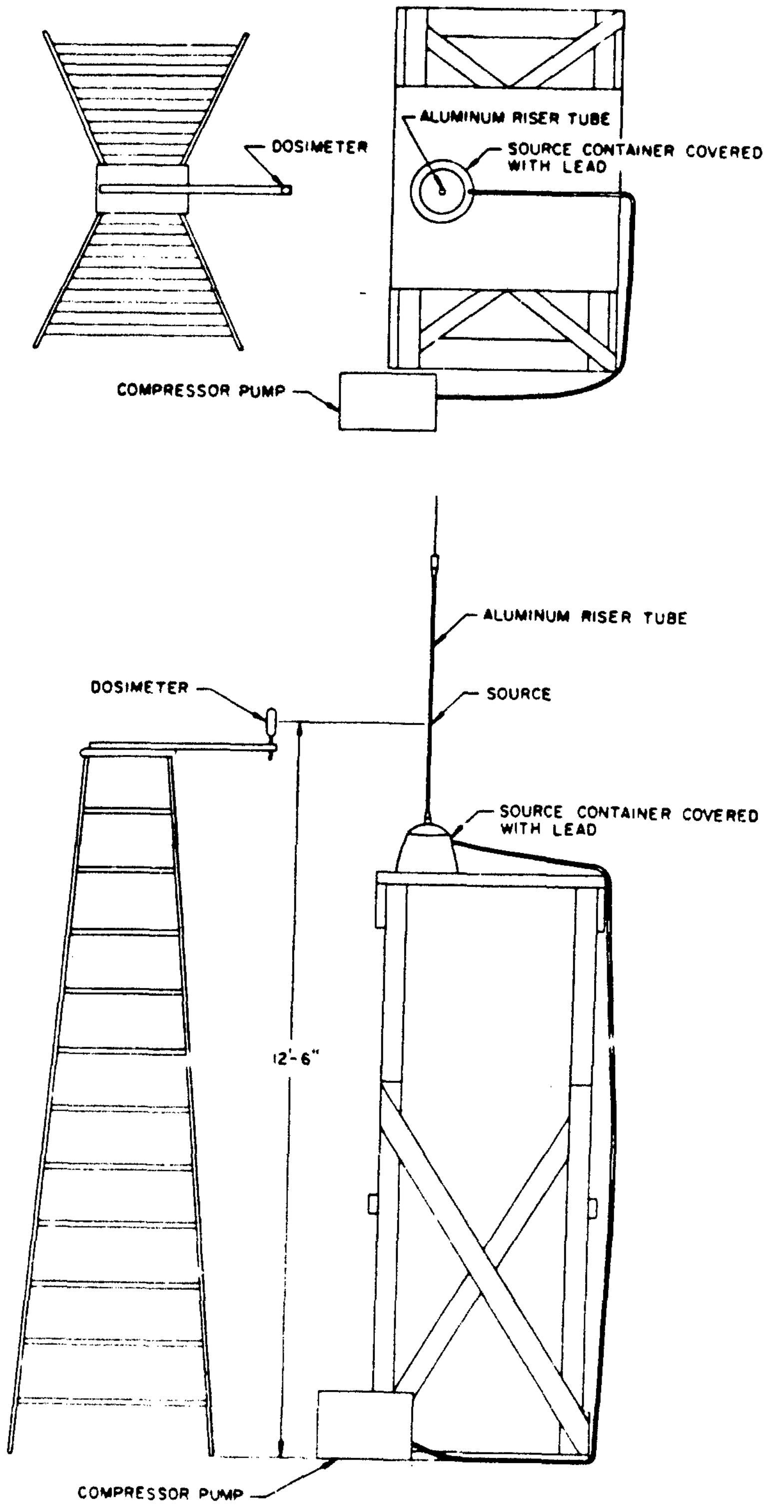

Figure B.1 Experimental set-up for calibration of stationary point sources.

K = air-ground interface buildup factor, and

μ = linear absorption coefficient in air at standard atmospheric conditions, 2.24×10^{-3} ft^{-1} for cobalt 60.

The effective curie strength of each source was determined by dividing the corrected exposure rate by the standard exposure rate for cobalt 60 (14.3 R/h per curie at a distance of 1 foot).

Table B.1 shows the effective curie strengths of the sources used in earlier experimentation as determined by the new method (C_N), along with the source strengths determined by the old method (C_o), corrected for radioactive decay. The maximum difference between the two is 1.6 percent, which is well within the error of ±3 percent inherent in the NBS calibrated standard.

Circulating point sources were calibrated similarly except that the plastic tubing was suspended above ground between two 12-foot-high stepladders spaced 6 feet apart (Figure B.2). A positive source stop was placed in the tubing line in a position that would stop the source halfway between the ladders. Radiation measurements were made with calibrated R chambers and the exposure rates were corrected to 1 foot by use of Equation B.1.

TABLE B.1 COMPARISON OF STATIONARY POINT SOURCE CALIBRATION DATA

Source Strength[a]	Distance x	B^b	K^b	$D_x{}^b$	$D_1{}^b$	Method $C_N{}^c$	Method $C_o{}^c$	Percent Difference
Ci	ft			R/h	R/h	Ci	Ci	
3.25	2	1.0039	1.0	5.37	21.39	1.50	1.509	0.53
3.25	4	1.0078	1.005	1.36	21.48	1.502	1.509	0.46
3.25	6.23	1.012	1.007	0.565	21.52	1.504	1.509	0.33
0.346	6.23	1.012	1.007	0.0612	2.33	0.163	0.161	0.62
94.5	2	1.0039	1.0	662	2638	186	183	1.6
94.5	4	1.0078	1.005	167	2631	184	183	0.5
94.5	6.23	1.012	1.007	71.4	2665	185	183	0.8

[a] Calibrated 1 September 1958.
[b] See Equation (B.1).
[c] Calibrated 1 September 1964.

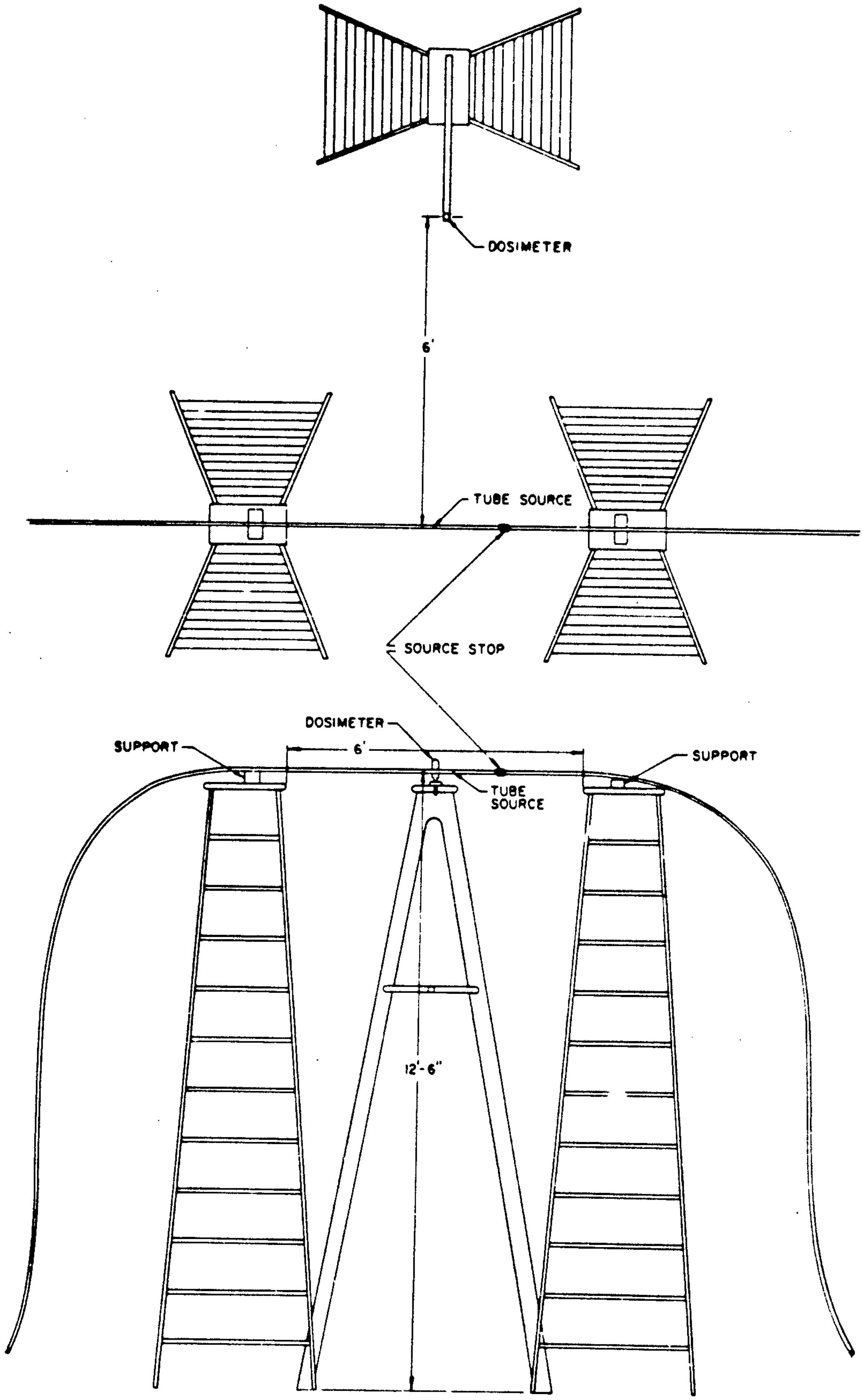

Figure B.2 Experimental set-up for calibration of circulating point sources.

APPENDIX C

FREE-FIELD EXPOSURE RATES MEASURED BY US ARMY NUCLEAR DEFENSE LABORATORY AND BY PROTECTIVE STRUCTURES DEVELOPMENT CENTER

One of the problems attendant with simulating a fallout field is that theoretically the fallout field is considered smooth and infinite in extent, a condition that is impractical to simulate. Therefore, the simulation of the field will be at best an approximation of the actual situation. This involves experimental measurements for a finite distance plus an analytical extrapolation for the far-field contribution. Earlier experiments measured the free-field exposure rates at the air-ground interface; cobalt-60 and cesium-137 sources were used to simulate the residual radiation (Reference 1). The site of these previous experiments was a relatively smooth, grassy field; however, the measurements were made with the source raised approximately 3-1/2 inches above the ground to ensure line-of-sight between source and detector and to reduce the effects of ground roughness in the measurements. These measurements were converted to ring-source data and the results were graphically integrated over the 800 feet covered by the measurements. An analytical estimate was made of the far-field contribution. The resultant infinite-field exposure rate at a 3-foot height was determined to be 497 R/h at a contamination density of 1 Ci/ft^2.

The 497 R/h compares favorably to the theoretical infinite-field exposure rate, 500 R/h, calculated by Eisenhauer (Reference 13). However, it was higher than the experimental infinite-field exposure rate, 464 R/h, determined by McDonnell, et.al., at the Protective Structures Development Center (PSDC), (Reference 10). Possible contributors to the difference in the above experimental exposure rates are (1) the method used to determine effective curie strengths of the sources and (2) ground roughness effects.

For the experiment in Reference 1, the sources were calibrated at a height of 11 feet above ground and at a horizontal distance of 6 feet from the detector. Measurements were made with and without an 8-inch-thick lead shield between the source and detector; the shield was designed to eliminate the direct radiation and to measure only the scattered radiation. These measurements resulted in a 5.1 percent correction for radiation-scatter contribution from the air-ground interface; this correction was applied in calculating the effective curie strengths of the sources. An objection to this method of source calibration was that the radiation scatter from the edges of the lead shield could be greater than the air-scattered radiation one is trying to measure. Subsequent measurements at a similar geometry indicated that the correction for the radiation scatter at the air-ground interface could be about 4.[illegible] percent too high.

To determine the validity of these source strengths, all the sources used in the previous experiment (Reference 1) were recalibrated under conditions closely approximating free-air conditions. Details of this recalibration are given in Appendix B. The recalibration indicated that the effective curie strengths of all sources were almost exactly as previously reported after corrections were made for decay.

Since the present measurements were being made with the point-source circulation system, which presented a different source geometry, a remeasurement of the free-field exposure rate was required. Because the surface had been graded and rolled, for practical purposes the field was considered a smooth, level plane. The free-field exposure rates at various heights above the field are shown in Table 3.1 and are presented graphically in Figure C.1. Curves showing the cumulative exposure rate for each annulus are plotted. These curves indicate the relative contribution for each annulus with increasing distance from the center of the field.

To compare the free-field data reported in Reference 1 with the free-field data obtained with the point-source circulation system (in this report), the cumulative exposure rates at the 3-foot height were plotted versus the distance from the center of the field in Figure C.2. Also shown in Figure C.2 are data measured at the 15-foot height (this report) and data at the 3-foot and 15-foot heights taken at PSDC (Reference 10). The curves at the 3-foot height show a definite difference between the previously taken NDL data (Reference 1) and the measured data in this report. The latter measurements were 5 percent lower than the previous measurements. The PSDC measurements were also lower (12 percent) at the 452-foot radius. The fact that the curves are very nearly parallel indicates that the difference in the exposure rates was probably due to differences in terrain (ground roughness) between the sites of the experiment. During the initial work (Reference 1), the source was exposed just above the surface of the field to decrease ground-roughness effects. However, the source was near enough to the ground to be considered at the air-ground interface without being extremely affected by the variations in the terrain. The circulating point source, on the other hand, travelled through plastic tubing that was laid directly on the ground. Although the surface had been graded and rolled, the field was only an approximation of a smooth field. That only an approximation of a smooth field can be achieved may be inferred from data obtained by Huddleston, et.al., (Reference 14) who, under somewhat similar conditions, made measurements of fallout radiation on a flat, dry lake bed at the Nevada Test Site. Angular distribution measurements 3 feet above ground resembled the theoretical curve at the 20-foot height above ground, or schematically as if the fallout on the ground has been covered with a mass thickness of material equivalent to 20 feet of air. This indicated that there are ground-roughness effects even on ground which appears to approach the ideal in smoothness in an infinite terrain.

Ordinarily it might be expected that the PSDC measurements in the free-field would be in closer agreement with the NDL measurements since similar systems were used to simulate the fallout areas. However, at the PSDC test site, washed gravel had produced a rolling terrain which introduced shadowing effects to the lower detectors; these were not present in the NDL measurements. This is substantiated in the close agreement of NDL and PSDC data at the 15-foot height.

The infinite-field exposure rate at a 3-foot height for this experiment was 468 R/h at unit curie density. This is approximately 5 percent lower than the exposure rate measured previously (Reference 1), a difference believed to be due primarily to ground roughness.

The experimental infinite-field exposure rates at heights to 15 feet taken at NDL and at PSDC are plotted in Figure C.3, along with the theoretical curve. The theoretical curve was calculated from Spencer's L(d) curve and a value of 468 R/h was assumed as the infinite-field value for a relatively smooth plane. The L(d) function is the total detector response at a distance d(in air) from an infinite, plane, isotropic source, divided by the total detector response at 3 feet in air from the same source. In general, the experimental free-field measurements of NDL and of PSDC agree very well with Spencer's theoretical values. Good agreement exists between the NDL measurements and the theoretical values near the ground, and the measurements above 5 feet agree within 3.8 percent; however, the PSDC measurements were low at the 1-foot and 3-foot detector heights. If it is assumed that the difference between the measurements at these low detector heights is due to ground roughness, a correction factor may be calculated for each height by obtaining a ratio of the theoretical-to-experimental exposure rate. When these ratios are applied for ground roughness correction to the PSDC cumulative results shown in Figure C.2, the agreement between NDL measurements and PSDC measurements becomes quite good. This is shown by the 3-foot height data in Table C.1.

TABLE C.1 COMPARISON OF THE PSDC FREE-FIELD EXPOSURE RATES CORRECTED FOR GROUND ROUGHNESS WITH NDL FREE-FIELD EXPOSURE RATES MEASURED AT THE 3-FOOT HEIGHT ABOVE AN INFINITE RADIATION FIELD SIMULATED BY COBALT 60

Outer Radius of Radiation Area	Cumulative Exposure Rates			Difference[c]
	Measured PSDC	Corrected[a] PSDC	Measured[b] NDL	
ft		(R/h)/(Ci/ft^2)		pct
17.9	159.4	174.9	-	-
32	213.4	234.1	-	-
68	279.1	306.2	297	3.1
164	344.6	378.0	370	2.2
452	398.6	437.3	438	0.2
∞	429.3	470.9	468	0.6

[a] Ground roughness correction factor = 1.097.

[b] Data at the indicated radii interpolated from Figure 4.2.

[c] $\text{Percent Difference} = \dfrac{\text{Corrected Exp Rate (PSDC)} - \text{Measured Exp Rate (NDL)}}{\text{Measured Exp Rate (NDL)}}$.

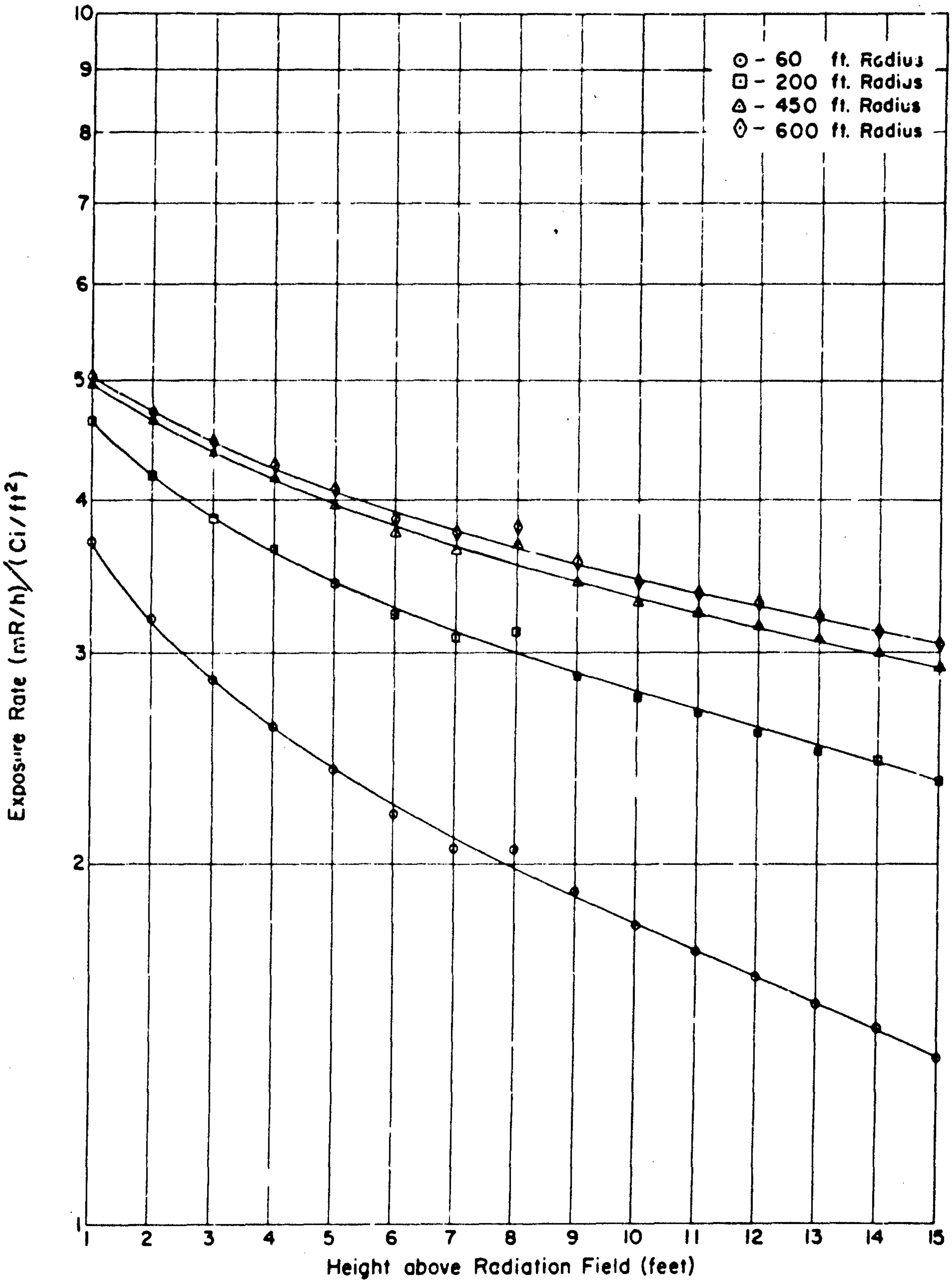

Figure C.1 Experimental exposure rates versus height above contaminated field.

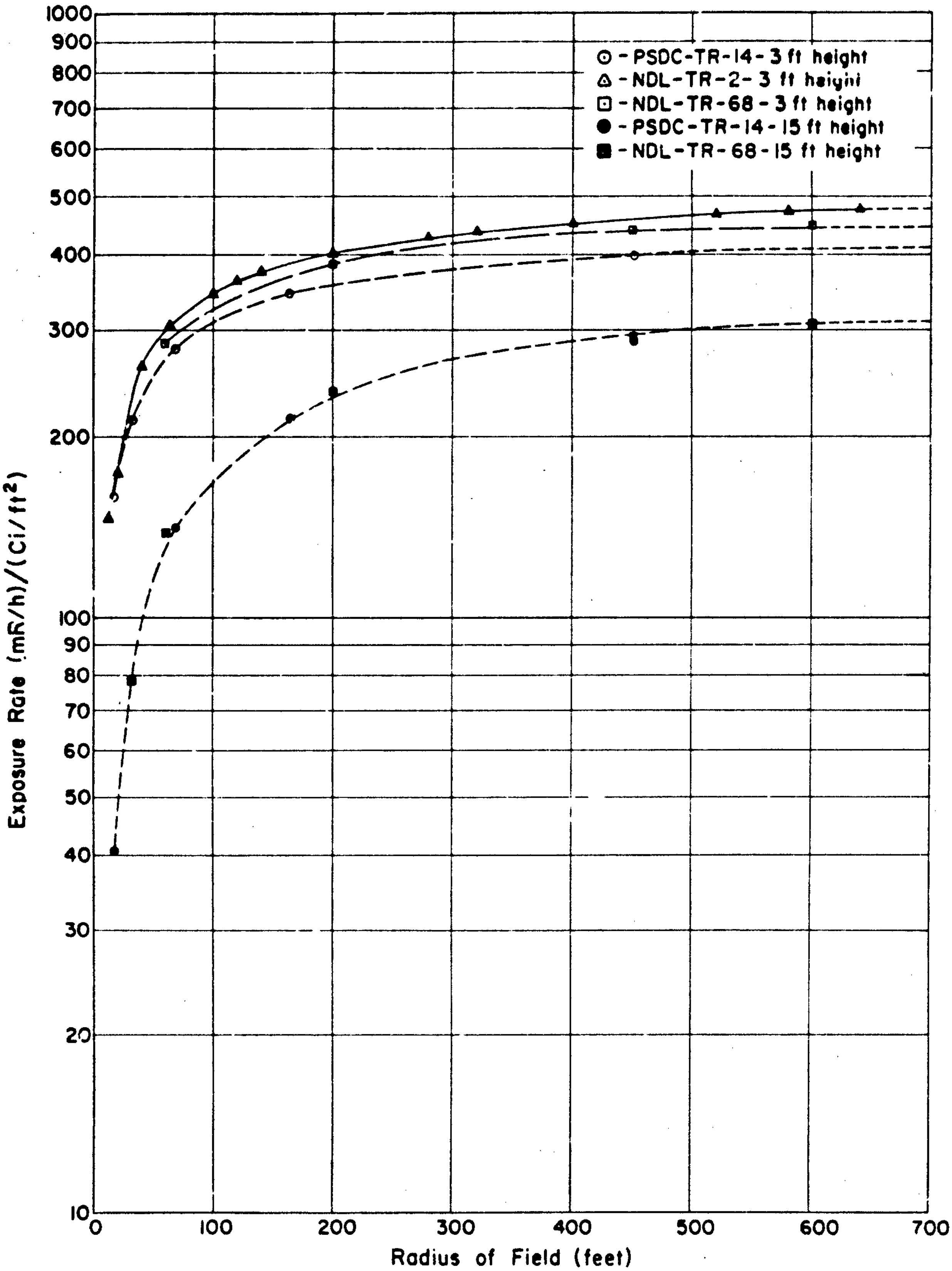

Figure C.2 Cumulative exposure rates versus radius of contaminated field as measured by NDL and PSDC.

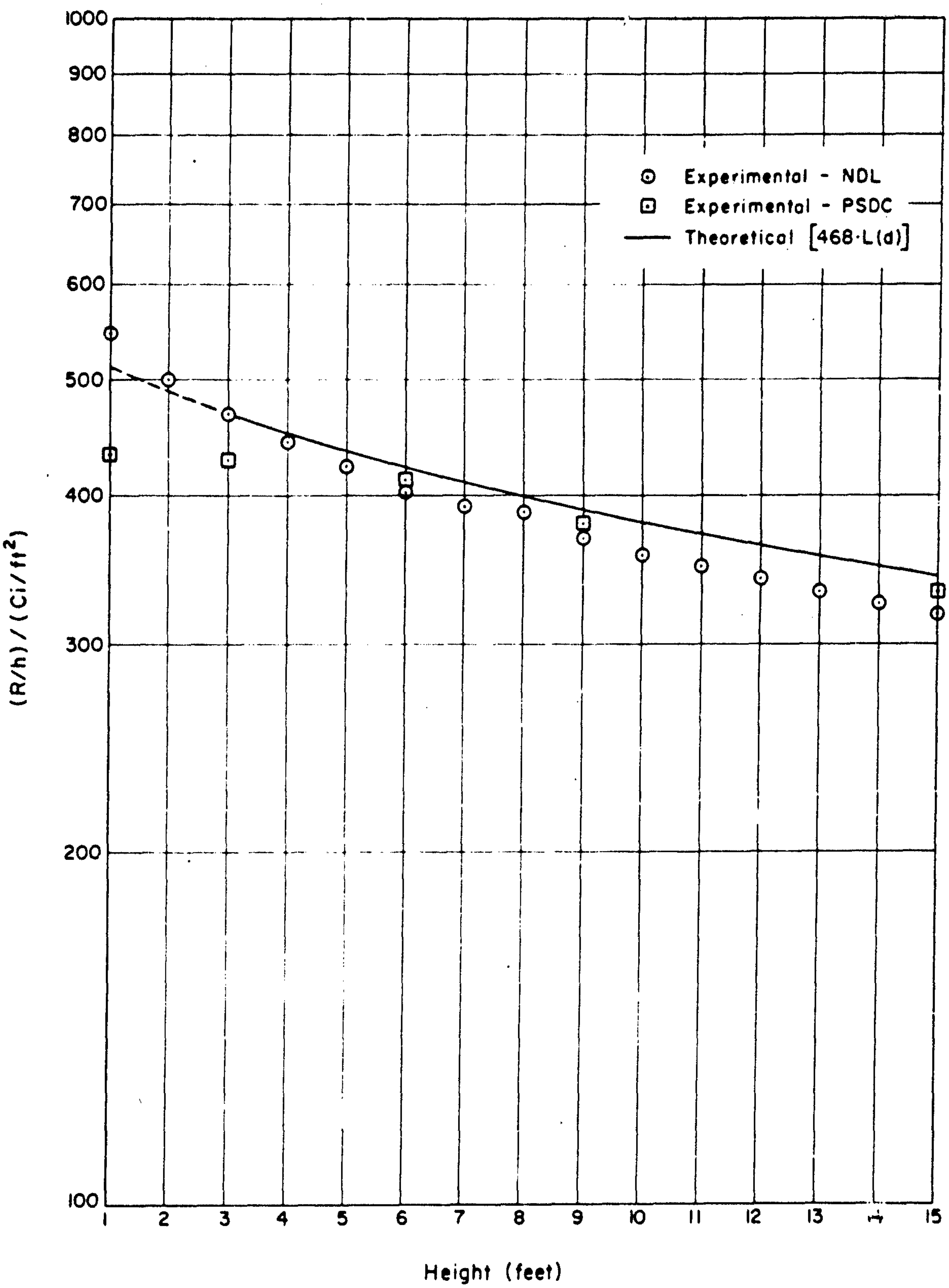

Figure C.3 Experimental and theoretical exposure rate versus height, d, above a radiation field.

DOCUMENT CONTROL DATA - R&D

(Security classification of title, body of abstract and indexing annotation must be entered when the overall report is classified)

1. ORIGINATING ACTIVITY *(Corporate author)* US Army Nuclear Defense Laboratory Edgewood Arsenal, Maryland 21010	2a. REPORT SECURITY CLASSIFICATION UNCLASSIFIED 2b. GROUP

3. REPORT TITLE

SCATTERED RADIATION (SKYSHINE)
CONTRIBUTION TO AN OPEN BASEMENT
LOCATED IN A SIMULATED FALLOUT FIELD

4. DESCRIPTIVE NOTES *(Type of report and inclusive dates)*

5. AUTHOR(S) *(Last name, first name, initial)*

Schumchyk, Michael J.
Schmoke, Murray A.
Egerland, Walter O.
Schulman, Ernest L.

6. REPORT DATE December 1966	7a. TOTAL NO. OF PAGES 78	7b. NO. OF REFS 14

8a. CONTRACT OR GRANT NO. b. PROJECT NO. OCD Work Order No. OCD-PS-64-91 c. Subtask No. 1111F d.	9a. ORIGINATOR'S REPORT NUMBER(S) NDL-TR-68 9b. OTHER REPORT NO(S) *(Any other numbers that may be assigned this report)*

10. AVAILABILITY/LIMITATION NOTICES

Distribution of this document is unlimited.

11. SUPPLEMENTARY NOTES	12. SPONSORING MILITARY ACTIVITY Office of Civil Defense

13. ABSTRACT

The objective of this work was to determine, experimentally, the shielding afforded by an open concrete-walled basement located in a simulated fallout field and to compare these experimental results with theoretical results published in National Bureau of Standards (NBS) Monograph 42.

A cobalt-60 point-source circulation system was used to simulate a uniformly-contaminated residual gamma radiation area out to a radius of 600 feet. Experimental exposure-rate measurements were made in the free field and at various locations within the structure as a function of height above the basement floor. Ionization chamber dosimeters were used as radiation detectors. Experimental measurements were extrapolated to infinite-field conditions by use of analytical procedures and compared with other related experimental data and theoretical results.

DD FORM 1 JAN 64 1473

14 KEY WORDS	LINK A		LINK B		LINK C	
	ROLE	WT	ROLE	WT	ROLE	WT
Fallout, Simulated						
Free-Field Exposure Rates						
Far-Field Exposure Rates						
Gamma Radiation						
Radiation, Gamma						
Radiation, Scattered						
Point-Source Circulation						
Cobalt-						
Skyshine						
Reduction Factors						
Basement, Open, Concrete						

INSTRUCTIONS

1. ORIGINATING ACTIVITY: Enter the name and address of the contractor, subcontractor, grantee, Department of Defense activity or other organization *(corporate author)* issuing the report.

2a. REPORT SECURITY CLASSIFICATION: Enter the overall security classification of the report. Indicate whether "Restricted Data" is included. Marking is to be in accordance with appropriate security regulations.

2b. GROUP: Automatic downgrading is specified in DoD Directive 5200.10 and Armed Forces Industrial Manual. Enter the group number. Also, when applicable, show that optional markings have been used for Group 3 and Group 4 as authorized.

3. REPORT TITLE: Enter the complete report title in all capital letters. Titles in all cases should be unclassified. If a meaningful title cannot be selected without classification, show title classification in all capitals in parenthesis immediately following the title.

4. DESCRIPTIVE NOTES: If appropriate, enter the type of report, e.g., interim, progress, summary, annual, or final. Give the inclusive dates when a specific reporting period is covered.

5. AUTHOR(S): Enter the name(s) of author(s) as shown on or in the report. Enter last name, first name, middle initial. If military, show rank and branch of service. The name of the principal author is an absolute minimum requirement.

6. REPORT DATE: Enter the date of the report as day, month, year, or month, year. If more than one date appears on the report, use date of publication.

7a. TOTAL NUMBER OF PAGES: The total page count should follow normal pagination procedures, i.e., enter the number of pages containing information.

7b. NUMBER OF REFERENCES: Enter the total number of references cited in the report.

8a. CONTRACT OR GRANT NUMBER: If appropriate, enter the applicable number of the contract or grant under which the report was written.

8b, 8c, & 8d. PROJECT NUMBER: Enter the appropriate military department identification, such as project number, subproject number, system numbers, task number, etc.

9a. ORIGINATOR'S REPORT NUMBER(S): Enter the official report number by which the document will be identified and controlled by the originating activity. This number must be unique to this report.

9b. OTHER REPORT NUMBER(S): If the report has been assigned any other report numbers *(either by the originator or by the sponsor)*, also enter this number(s).

10. AVAILABILITY/LIMITATION NOTICES: Enter any limitations on further dissemination of the report, other than those imposed by security classification, using standard statements such as:

(1) "Qualified requesters may obtain copies of this report from DDC."

(2) "Foreign announcement and dissemination of this report by DDC is not authorized."

(3) "U. S. Government agencies may obtain copies of this report directly from DDC. Other qualified DDC users shall request through
______________________________."

(4) "U. S. military agencies may obtain copies of this report directly from DDC. Other qualified users shall request through
______________________________."

(5) "All distribution of this report is controlled. Qualified DDC users shall request through
______________________________."

If the report has been furnished to the Office of Technical Services, Department of Commerce, for sale to the public, indicate this fact and enter the price, if known.

11. SUPPLEMENTARY NOTES: Use for additional explanatory notes.

12. SPONSORING MILITARY ACTIVITY: Enter the name of the departmental project office or laboratory sponsoring *(paying for)* the research and development. Include address.

13. ABSTRACT: Enter an abstract giving a brief and factual summary of the document indicative of the report, even though it may also appear elsewhere in the body of the technical report. If additional space is required, a continuation sheet shall be attached.

It is highly desirable that the abstract of classified reports be unclassified. Each paragraph of the abstract shall end with an indication of the military security classification of the information in the paragraph, represented as *(TS)*, *(S)*, *(C)*, or *(U)*.

There is no limitation on the length of the abstract. However, the suggested length is from 150 to 225 words.

14. KEY WORDS: Key words are technically meaningful terms or short phrases that characterize a report and may be used as index entries for cataloging the report. Key words must be selected so that no security classification is required. Identifiers, such as equipment model designation, trade name, military project code name, geographic location, may be used as key words but will be followed by an indication of technical context. The assignment of links, rules, and weights is optional.